Electronic correlations and disorder in transport through one-dimensional nanoparticle arrays

E. Bascones,[1,2,3,*] V. Estévez,[1] J. A. Trinidad,[2] and A. H. MacDonald[2]
[1]*Instituto de Ciencia de Materiales de Madrid, CSIC, Cantoblanco, E-28049 Madrid, Spain*
[2]*Department of Physics, University of Texas at Austin, Austin, Texas 78712, USA*
[3]*Theoretische Physik, ETH-Hönggerberg, CH8050 Zurich, Switzerland*
(Received 24 September 2007; revised manuscript received 22 May 2008; published 18 June 2008)

We report on a detailed study of the transport properties of one-dimensional metallic nanoparticle arrays, which focuses on threshold voltages and on the spatial distribution of potential drops across the array both below and above thresholds. We study dependences on array parameters and analyze the roles of charge and resistance disorder. We consider the case in which the interaction between charges is local and the case of long-ranged interactions separately. We show that some of the differences between the transport properties of arrays with short and long-range interactions are due to interactions between charges in different nanoparticles, while others are due to interactions between charges in the islands and those at the electrodes, which produce a polarization potential drop through the array. Finally we study how strong disorder due to charged impurities trapped in the substrate is partially screened by redistribution of charges among the nanoparticles and demonstrate that long-range interactions induce correlations in the screened disorder potentials of neighboring islands.

DOI: 10.1103/PhysRevB.77.245422 PACS number(s): 73.23.Hk, 73.23.−b, 73.63.−b

I. INTRODUCTION

Arrays made of metallic,[1–10] semiconducting,[10–16] magnetic[17–19] or mixed property[20–22] nanoparticles with radii of ~2–7 nm can be now synthesized. The transport properties of these systems are influenced by the ratios between the energy level spacing, the charging energy of the nanoparticles, and the temperature. The first two quantities depend on the material and the size of the nanoparticle. In the case of metallic nanoparticles, at not too low temperatures, the level spacing is much smaller than the temperature and does not play any role in the transport.[23] On the contrary, the charging energy is of the order of 0.1 eV. Strong interactions between the electric charges and the possibility of tuning interparticle coupling make nanoparticles arrays an ideal system to study correlated motion.[24–44]

Experimentally, these arrays are strongly influenced by disorder.[45–47] Local charging disorder is present in all arrays due to randomly dispersed charged impurities lodged in the substrate or in the materials that separate and surround the nanoparticles. Because of the exponential dependence of the tunneling resistance, even a small dispersion in the distance between nanoparticles results in large variations in the tunneling resistances of the junctions. Differences in the island sizes and voids in the lattice can be other sources of disorder.[3]

Due to the combination of disorder and charging effects the current in voltage biased arrays is blocked up to a threshold voltage[31,35,45,48–54] V_T. For bias voltages larger than V_T, the current is in general nonlinear in voltage with a power-law dependence[45,51,55] close to threshold, a linear dependence recovered at high-voltages, and frequently a steplike behavior, called a Coulomb staircase, at intermediate voltages.

In spite of the effort done in the last two decades, the transport properties of these systems are not completely understood. Most studies have focused on the statistical analysis of the threshold voltage and on the power-law behavior of the current close to this threshold. This exponent depends on the dimensionality of the array, but there is controversy between different theoretical approaches in the one-dimensional case with both linear[31,35,56] and square-root[57] predictions. Much experimental work has been concentrated on two- and three-dimensional arrays, but some quasi-one-dimensional systems have also been fabricated.[4,6,51] Comparison between experiments and theory is not yet well settled.

Theoretical analysis have mainly considered arrays in which each nanoparticle is capacitively coupled only to its nearest neighbors,[31,35,48,52–54,56] especially the case in which this coupling is small. The truncation of capacitive coupling to nearest-neighbor results in an interaction between charges in different conductors, which decays exponentially with the distance between them.[31,48] This limit is relevant for those arrays coupled to a gate electrode[55] as the mobile charges in the gate electrodes effectively screen Coulomb interactions. Self-assembled arrays fabricated nowadays are deposited onto insulating substrates and generally lack a gate voltage. In these arrays, the screening of long-range interactions is less effective, but the proximity of other conductors, both islands and leads, modifies its value compared to a $1/r$ Coulomb law.[69,70] The electrodes contribute to the screening of the interaction. Theoretical analysis including the effect of long-range interactions is scarce and limited[35,49,57] to numerical results or particular cases.

In this paper, we provide a complete description of the zero-temperature transport properties of one-dimensional metallic nanoparticle arrays. We discuss arrays with and without charge disorder. Although clean arrays are mainly of academic interest, their analysis will help us to understand the main features of the experimentally more relevant disordered arrays. The effect of variations in the junction resistances is also analyzed. Disorder in capacitances (nanoparticle size variations) is not considered as it is less important in present experiments. Nanoparticles synthesized nowadays are monodispersed in size to a few percent. In any case, the effect of capacitance disorder[58] in most of the properties

studied here can be deduced from the analytic approximations provided in the text. Due to the one dimensionality of the array and the nearest-neighbor tunneling considered, we assume that there are no nanoparticle voids in the array, as this would completely prevent current flow. Interactions are introduced via an inverse capacitance matrix. We consider both the case in which interactions are restricted to charges in the same nanoparticle (onsite limit) and the effect of the long-range character of the interactions. In the last case, the inverse capacitance matrix is calculated including the effect of screening.

We have analyzed the threshold voltage, the *I-V* characteristics, not only close to threshold but also at larger bias voltages and the potential drop through the array. We identify an asymmetry external parameter α, which controls the bias voltage drop. The influence of α has barely been discussed in previous works. Calculations are performed numerically, but analytic approximations are given in several limits and compared with numerical results.

The paper is organized as follows: In Sec. II we describe the system and model under study. This section is divided into three subsections. In Sec. II A we describe the system under consideration and define the parameters used. Section II B introduces the concepts of excitonic energy, potentials and the islands and junctions, and, in particular, the polarization potential. These concepts will be used in the discussion of the transport properties. Section II C describes the Monte Carlo simulation used in the calculation of the *I-V* curves. Section III discusses the threshold, *I-V* curves, and potential drop characteristic of arrays with on-site interactions. Sections IV and V are dedicated to long-range interactions. Section IV summarizes the main results obtained for the shape of the interaction in the long-range case and discusses the correlations induced in the screened disorder by the long-range character of the interaction, while in Sec. V we discuss the transport properties. A summary of the main results is given in Sec. VI. Readers who are not interested in the technical details can go directly to Sec. VI. In the Appendix the methods used to compute the long-range interaction including screening are explained.

II. MODEL

A. System under consideration

We consider a one-dimensional array composed of N metallic spheres of radius r^{isl} and center to center distance $2r^{isl}+d$. Throughout lengths are measured in units of r^{isl} and energies in units of $E_c^{isl}=e^2/(2C^{isl})$, the charging energy of an isolated nanoparticle having capacitance C^{isl}. Here and in the following, the electronic charge $e=1$. To analyze the transport the array is sandwiched between two large electrodes. We consider the classical Coulomb blockade regime with $\delta \ll K_BT < E_c^{isl}$. δ is the level spacing and T is the temperature. We assume that each nanoparticle has a continuum level spectrum ($\delta=0$) and a constant density of states at the Fermi level but a gap E_c^{isl} for adding charge.

The nanoparticles are separated by high tunneling barriers with a resistance much larger than the quantum of resistance. In these conditions the charge in the islands can be assumed fixed and quantized. Eventually we allow tunneling processes between nearest neighbors and treat the transport at the sequential tunneling level. A single charge is involved in the tunneling process. We assume that when a charge hops, the charge density in the final state of the array immediately relaxes to the electrostatic equilibrium configuration. The probability of a tunneling process[23] is given by

$$\Gamma(\Delta E) = \frac{1}{R}\frac{\Delta E}{\exp(\Delta E/K_BT)-1} \tag{1}$$

with R as the tunneling resistance of the junction.

Whenever not specified we assume that all the junction resistances R_i are equal and given by R_T. The effect of nonhomogeneous resistances will be studied in two ways. One of the junction resistances at a given position is larger than the other ones (given by R_T) or resistances, varying in between two values are randomly assigned to the junctions. To mimic that disorder in resistances originates in variations in distances between the islands and the exponential dependence of the junction resistance on the distance between islands, the junction resistance is given by $R=R_0\exp(\gamma \text{dist})$, with R_0 and γ as the input parameters and dist$=1+$random$/2$. Here *random* is a random number between 0 and 1. In this paper, we have used $R_0=1.1825R_T$ and $\gamma=1.526, 1.95, 2.84$. With these values the resistance changes, respectively, between $(5-11)R_T$, $(8-21)R_T$, and $(23-83)R_T$.

We will restrict the discussion to zero temperature for which $\Gamma(\Delta E)=-\Delta E/R\Theta(-\Delta E)$. ΔE is the difference between the energy of the system before and after the tunneling event, with the sign convention that ΔE is negative if the energy decreases. The energy gained by tunneling is assumed to be dissipated. Only changes in energy with electrostatic origin are considered.

The energy of the system is given by

$$F = \frac{1}{2}\sum_{\gamma,\beta=0}^{N+1} Q_\gamma C^{-1}_{\gamma\beta} Q_\beta + \sum_{i=1}^{N} Q_i \phi_i^{\text{dis}}. \tag{2}$$

Labels 0 and $N+1$ refer to source and drain electrodes and $1,\ldots,N$ to the islands. Latin capital and lower case letters are used to denote electrodes and islands, respectively. Greek indices will be used when the labels refer to both islands and electrodes. Q_γ is the charge present in the conductor. Charges Q_0 and Q_{N+1} maintain source and drain electrodes at potentials V_0 and V_{N+1}, respectively. The electrostatic interactions in our system are defined through an inverse capacitance matrix C^{-1}. All the elements $C^{-1}_{\gamma,\beta}$ are positive. The inverse capacitance matrix is symmetric, $C^{-1}_{\gamma\beta}=C^{-1}_{\beta\gamma}$, and has dimension $(N+2)\times(N+2)$, i.e., it includes both islands and electrodes. The coupling between the islands and the electrodes is included through $C^{-1}_{i,K}$ and $C^{-1}_{K,i}$.

For the interactions, we consider two cases. In the limit referred to as short-range or on-site interaction, we restrict electrostatic interactions to those charges on the same conductor: capacitive coupling between different conductors and all nondiagonal matrix elements $C^{-1}_{\gamma,\beta}$ ($\gamma\neq\beta$) vanish and $C^{-1}_{ii}=C^{-1}_{i}=C^{-1}_{isl}$. In the so-called long-range limit, the interaction potential differs from the $1/r$ Coulomb dependence, as in $C^{-1}_{\gamma,\beta}$ we take into account the static screening due to the

presence of other conductors. For simplicity to describe the electrodes, we have considered two large spherical leads. To obtain the screened interaction potential, we have developed two numerical methods to calculate the inverse capacitance matrix of an array of spheres. These methods are explained in the Appendix. The modification of the interaction with respect to the $1/r$ law due to the presence of the other nanoparticles is discussed in Sec. IV. The on-site interaction limit can be compared with $d/r^{isl} \to \infty$ as the particles are so far apart that the interaction between charges in different conductors can be neglected. As closer are the particles, more important is the interaction between charges in them. Experimentally, $d/r^{isl} \sim 0.5$.

ϕ_i^{dis} is a random potential at each island due to randomly dispersed charges within the substrate and within the material surrounding the nanoparticles.[59] Clean arrays will be characterized by $\phi_i^{\mathrm{dis}}=0$ for every i. The random potential is included only at the islands because a similar term at each electrode is compensated by the battery and thus has no effect on transport. In the case of disordered arrays, the disorder potentials can, in principle, take values larger than the charging energy E_c^{isl}. However, for large values of the disorder potential, charges flow to compensate for these large fluctuations. In the case of short-range interactions, except if the original disorder potential is very weak, once the screening of the potential due to the mobile charges is taken into account, the set of disorder potentials is uniformly distributed in the interval $-E_c^{isl} \leq \phi_i^{\mathrm{dis}} \leq E_c^{isl}$.[45] The distribution of the disorder potential in the long-range limit is discussed in Sec. IV B.

We take into account that the electrodes are not ideal voltage sources but have a finite self-capacitance. In equilibrium and before the tunneling event, the electrodes are held at a given potential due to the charge provided by a battery. We assume that the tunneling time, i.e., the time needed by the electron to cross the tunnel barrier, is smaller than the circuit characteristic time that determines how quickly the battery can transfer charge to the leads in order to restore the voltage at the electrodes. As a consequence, just after the tunneling process the electrodes will not necessarily be at the same potential at which they were at before the tunneling event because the charge, provided by the battery, necessary to restore their initial potentials has not arrived yet. The voltage is restored to the nominal value before the next tunneling event. For finite-range interactions, the potentials on the leads will thus fluctuate in response to all tunneling events, even those that do not directly involve the electrodes. In the short-range case, they will fluctuate only when an electron jumps into or out of the leads.

In the following we rewrite the potential at the electrodes as $V_0=\alpha V$ and $V_{N+1}=(\alpha-1)V$. The total potential drop through the array is $V_0-V_{N+1}=V$. Some measurable properties depend on the value of α, which characterizes how the bias voltage is partitioned between source and drain chemical-potential shifts. In several previous works, the value of α was chosen either as $\alpha=1/2$, correspondingly to a symmetrically biased array, or as $\alpha=0,1$, corresponding to completely asymmetric biasing. $\alpha=1$ has been also called the forward bias condition.[60] Both values have been used in the literature, mostly without discussion. In the symmetrically biased case, the potential drop at both contact junctions is equally modified by the bias voltage. On the contrary for $\alpha=0(1)$ only the drain (source) junction is affected by the bias. Since no physical properties depend on the overall zero of energy, varying α in our model is entirely equivalent to rigidly shifting all impurity potentials by $-\alpha V$. The dependence on α discussed below, corresponds in part to a dependence on the alignment of the equilibrium source and drain chemical potentials with respect to the addition and removal energies of the electron. For example, for a single nanoparticle on whether the chemical-potential shift required to add or remove an electron is larger. Since in our model all transport occurs by transfer between adjacent nanoparticles, the evolution of a nanoparticle array as the bias voltage is applied is sensitive to α. For a given nanoparticle array with a fixed set of disorder potentials, we believe that the dependence on α discussed below should in principle be observable.

B. Potential at islands and junctions

The relevant quantity for the transport is the change in energy due to a tunneling event. The tunneling process can be seen as the creation of a hole in the conductor γ from which the charge leaves, $Q_\gamma \to Q_\gamma - 1$, and the addition of an electron in β at which the charge arrives, $Q_\beta \to Q_\beta + 1$. Here and thereafter, we let $+1(-1)$ denote the charge of an electron (hole). The change in energy can be rewritten as

$$\Delta E = E_{\gamma,\beta}^{e-h} + (\phi_\beta - \phi_\gamma). \tag{3}$$

The first term gives the energy to create an electron-hole pair (also called in the following excitonic energy) in an uncharged clean array and is given by

$$E_{\gamma,\beta}^{e-h} = \frac{1}{2}C_{\gamma\gamma}^{-1} + \frac{1}{2}C_{\beta\beta}^{-1} - C_{\gamma\beta}^{-1}. \tag{4}$$

This energy does not depend on the direction of tunneling (from γ to β or from β to γ), and in the following, it will be denoted by E_i^{e-h} with i running from 1 to $N+1$. The index i, when used to label a junction, will refer to the one between conductors $i-1$ and i. We will use the term *contact* junction for those junctions, which connect an island and an electrode, and *bulk* or inner junction for those ones in between two nanoparticles. In the short-range case,

$$E_{\gamma,\beta}^{e-h} = \frac{1}{2}C_{\gamma}^{-1} + \frac{1}{2}C_{\beta}^{-1}. \tag{5}$$

For the contact junctions $i=1,N+1$, $E_i^{e-h} \sim E_c^{isl}$ as $E_c^{\mathrm{source,drain}} \ll E_c^{isl}$, while for the bulk junctions $i=2$ to $i=N$, $E_i^{e-h}=2E_c^{isl}$.

The second term in Eq. (3) can be seen as the change in potential between the conductors involved in the tunneling. The potential at each site depends on the charge state of the array prior to the tunneling event, which at the electrodes is $\phi_0=V_0=\alpha V$, $\phi_{N+1}=V_{N+1}=(\alpha-1)V$. At the islands the potential can be decomposed into three terms $\phi_i=\phi_i^{\mathrm{dis}}+\phi_i^{\mathrm{pol}}+\phi_i^{\mathrm{ch}}$: the disorder potential ϕ_i^{dis} due to random charges in the substrate, the polarization potential ϕ_i^{pol} at the island induced by the electrodes at finite bias, and the potential due to the

charges in the nanoparticles ϕ_i^{ch}. In the short-range case the polarization potential ϕ_i^{pol} at the islands vanishes. For long-range interaction, it is given by

$$\phi_i^{\mathrm{pol}} = \lambda_i^{\alpha} V, \tag{6}$$

with

$$\lambda_i^{\alpha} = C_{\mathrm{gen}}^2 [\alpha (C_{i0}^{-1} C_{N+1,N+1}^{-1} - C_{i,N+1}^{-1} C_{N+1,0}^{-1}) + (\alpha - 1)(C_{iN+1}^{-1} C_{00}^{-1} - C_{i0}^{-1} C_{N+1,0}^{-1})], \tag{7}$$

and

$$C_{\mathrm{gen}}^2 = \frac{1}{C_{00}^{-1} C_{N+1,N+1}^{-1} - (C_{N+1,0}^{-1})^2}. \tag{8}$$

In the short-range limit, the charging potential equals

$$\phi_i^{\mathrm{ch}} = \frac{Q_i}{C_i}, \tag{9}$$

while for long-range interactions it is given by

$$\phi_i^{\mathrm{ch}} = \sum_{j=1}^{N} Q_j \tilde{C}_{ij}^{-1}, \tag{10}$$

with

$$\tilde{C}_{ij}^{-1} = C_{ij}^{-1} + C_{\mathrm{gen}}^2 [C_{0,N+1}^{-1} (C_{iN+1}^{-1} C_{j0}^{-1} + C_{i0}^{-1} C_{j,N+1}^{-1}) - C_{00}^{-1} C_{N+1,i}^{-1} C_{j,N+1}^{-1} - C_{N+1,N+1}^{-1} C_{i0}^{-1} C_{j0}^{-1}], \tag{11}$$

with C_{gen} given by Eq. (8). $\tilde{C}^{-1}$ can be interpreted as a modification of the interaction between the charges in the islands due to the proximity of the electrodes at a fixed potential. For the case $i=j$ in which both charges are on the same island this modification was already discussed in Ref. 48, as the interaction of a soliton with a passive edge. Expression (11) shows that not only when the charges are in the same island but also when they occupy different islands, their effective interactions are modified by the presence of the voltage-biased leads. Two types of terms can be differentiated in the modification of this interaction. The last two terms in Eq. (11), or direct terms, can be viewed as the interaction between a charge in island i and the image charge at one of the electrodes induced by the charge in island j. This term is affected by the presence of the other electrode. On the other hand, the terms containing C_{0N+1}^{-1}, or indirect terms, reflect the interaction between the image charges in both electrodes. Direct and indirect terms have opposite sign. The direct term reduces the effective interaction; the indirect one increases it.

Equations (3)–(11) follow from Eq. (2) after straightforward and trivial algebra. For further convenience, we have just defined a few quantities and split the change in energy ΔE and potential ϕ_α. Analogously we can define the potential drop at each junction,

$$\Phi_i = \phi_i - \phi_{i-1}, \tag{12}$$

with the corresponding polarization, disorder, and charging terms Φ_i^{pol}, Φ_i^{dis}, and Φ_i^{ch}. At a given junction,

$$\Phi_i^{\mathrm{pol}} = \Lambda_i^{\alpha} V = (\lambda_i^{\alpha} - \lambda_{i-1}^{\alpha}) V. \tag{13}$$

Here $\lambda_0^{\alpha} = \alpha$ and $\lambda_{N+1}^{\alpha} = \alpha - 1$. In the short-range case ($\lambda_i^{\alpha} = 0$, for $i=1$ to N), the potential drop at a bulk junction does not depend on the bias voltage or α, except via a change in the charge state.

C. Numerical simulation

The current is calculated numerically by means of a Monte Carlo simulation,[48] which depends on the tunneling rates. The state of the array consists of the set of charges $\{Q_\beta\}$ that occupy the array islands and the leads. The charges in the leads keep the leads at voltages V_0 and V_{N+1}.

At each iteration a single tunneling event takes place. The time involved in this event τ depends on the tunneling rates of all the possible tunneling processes. First, it is computed the change in energy and the tunneling rate of the $2(N+1)$ possible hopping events, corresponding to the tunneling of a single electron, to the left or to the right, through any of the $(N+1)$ junctions. The probability of changing the initial configuration varies with time like

$$P^{\mathrm{change}}(t) = 1 - P^{\mathrm{stay}}(t) = 1 - e^{-\Gamma^{\mathrm{tot}}(t - t_0)}, \tag{14}$$

with t_0 as the time at which the preceding tunneling process took place and $\Gamma^{\mathrm{tot}} = \Sigma_{i=1}^{N+1} (\Gamma_i^+ + \Gamma_i^-)$. Γ_i^+ and Γ_i^- are the tunneling rates through the i junction to the left or to the right, respectively, and are calculated from Eq. (1). To sample the time interval between two hopping events, we generate random numbers between [0,1] to mimic P^{change} and obtain $\tau = t - t_0$ from Eq. (14). As the average of $-\ln P^{\mathrm{stay}}$ is the unity, if one is interested only in the average values of the charge or the current, and not on its fluctuations, the time step τ could be fixed[68] to $1/\Gamma^{\mathrm{tot}}$. This option is numerically faster.

The relative probability of each tunneling event is $\Gamma_i^{\pm}/\Gamma^{\mathrm{tot}}$. To determine the hopping process, which changes the charge state, the relative probabilities are consecutively arranged in the interval [0,1]. A second random number in this interval is generated to select the tunneling process. Then, the charge configuration is updated. After we modify the state of the system, we allow the external circuit to return the leads to their applied bias values prior to the selection of the next hop. This effect is simulated by resetting the charges on the source and the drain to the values that restore the nominal applied bias.

In order to remove all sensitivity to initial conditions before we track the evolution of $\{Q_i\}$ as a function of time at any voltage, we perform $N_{\mathrm{eq}} \geq 10^4$ iterations to equilibrate the system. Following these iterations, we track the evolution of the charge state until the net number of electrons that arrive at the drain, Q_{drain}, equals a very large number ($\geq 10^5$). The average calculated current is given by

$$I = \frac{Q_{\mathrm{drain}}}{t_{\mathrm{tot}}}, \tag{15}$$

where t_{tot} is the sum of all time intervals between hopping processes in the evolution runs. If a tunneling event involving the drain is selected, an amount $\delta q = \pm 1$ is added to Q_{drain} depending on whether an electron hopped to or from

the drain. Current conservation ensures that the average current is the same through any junction. The minimum numbers of equilibration cycles, N_{eq}, and evolution cycles (set by Q_{drain}) depend on the voltage. To calculate the average voltage drop, we assume that the system is in a given state a time equal to the interval τ until the next tunneling event takes place.

III. SHORT-RANGE INTERACTION

A. Threshold voltage

The threshold voltage is the minimum bias voltage at which current can flow through the array. It is controlled by the changes in energy in tunneling and not affected by the resistance of the junctions; thus, we do not address the case of disorder in resistance in this section. A finite current requires that charges are able to be transferred from one electrode to the other one across the entire array. If charge flow can occur between the leads, the threshold voltage is the minimum voltage that permits the entrance of an electron or hole into the array. A finite bias voltage can assist the entrance of charge to the array from the leads, as it creates a potential drop at the contact junction, which can overcome the excitonic energy. However, it is possible for charge to become stacked inside the array due to the disorder potential configuration or due to the lack of potential drops across the bulk junctions.

At strictly zero temperature, the tunneling rate $\Gamma(\Delta E) = \frac{-1}{R_T}\Delta E\Theta(-\Delta E)$ and vanishes when ΔE is positive or zero. In the on-site limit, in the case of clean arrays at the inner junctions ΔE is independent of the bias voltage and zero or positive if the two islands differ just by just a single charge. $N-1$ junctions, with zero tunneling rate, prevent the flow of charges. A charge gradient at each bulk junction has to be created to allow flow of charge. The threshold corresponding to the clean case is plotted in Fig. 1(a) for the case of symmetrically biased arrays ($\alpha=1/2$), antisymmetrically biased arrays ($\alpha=1$), and an intermediate biasing ($\alpha=3/4$). In the symmetrically biased case, V_T shows a steplike dependence on N and even-odd effect. In this case, increasing the potential at the electrodes allows positive and negative charges to enter from the source and the drain respectively. These charges accumulate on the array and create potential drops across the bulk junctions. At voltages just below the threshold, the accumulated charges at the first and last islands are equal in number and opposite in sign. Current starts to flow at voltages larger than $V_T=2NE_c^{isl}$ when N is odd and $V_T=2(N-1)E_c^{isl}$ when N is even. These values allow for the build up of $\pm(N-1)/2$ and $\pm(N-2)/2$ charges at the first and last islands for odd and even N, respectively, creating a charge gradient $dQ_i=Q_i-Q_{i-1}=-1$ across all bulk junctions for odd N and across all bulk junctions except one for even N.

The even-odd effect is absent for $\alpha=1$ and $\alpha=0$ with a threshold voltage $V_T=E_c^{isl}(2N-1)$. For $\alpha=0,1$, charge can only enter the array from one lead and the energy barriers across *all* $N-1$ bulk junctions must be overcome by accumulated charges. When $\alpha=1/2$ the first and last junctions are equivalent and charge can enter from both leads so it is possible in some cases for the energy barrier across one of the bulk junctions to be overcome by the potential drop due to two injected charges of opposite sign from the two leads, i.e., one of the junctions can be uncharged. The absence of this possibility is what removes the even-odd effect when $\alpha=0$ and $\alpha=1$. An intermediate situation is found for $\alpha=3/4$.

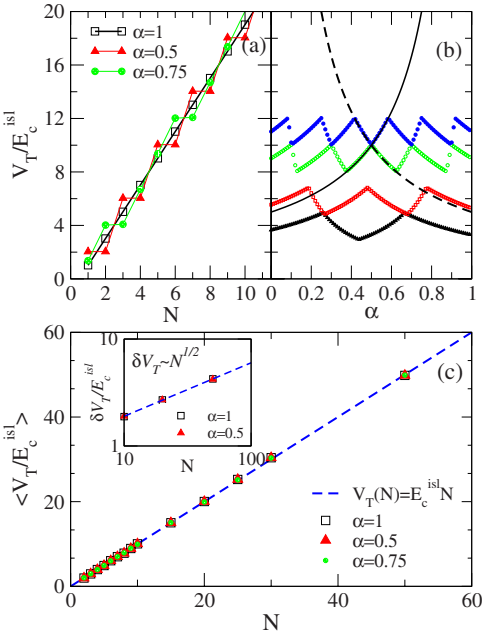

FIG. 1. (Color online) (a) Threshold voltage of clean arrays as a function of the number of islands N for different values of the asymmetry bias parameter α. A clear even-odd effect is present for symmetrically biased arrays, $\alpha=1/2, (V_0=V/2=-V_{N+1})$. (b)Threshold voltage as a function of α. From top to bottom lines with symbols correspond to clean arrays with six and five islands and to disordered arrays with six and five islands. For comparison, the thin solid and dashed lines give, for clean arrays, the bias voltage at which 2 and −2 charges can be placed at the first and last islands. (c) Main figure: average threshold voltage for disordered arrays as a function of the number of islands. The dependence of V_T on α disappears on average and a linear dependence on N is recovered. Fluctuations in threshold voltage follow $\delta V_T \sim N^{1/2}$ as predicted (Ref. 31).

For given N the threshold voltage changes in a periodic way with α [see Fig. 1(b)], with a period dependent on the number of barriers in the array. Dependence of V_T on N and periodic features in V_T with respect to α reflect the number of charges, which have to accumulate in the first and last island prior to current flow. Figure 1(b) includes curves corresponding to V_0 and V_{N+1} for specific values of Q_1 and Q_N. With increasing bias asymmetry (increasing $|\alpha-1/2|$), the threshold voltage is alternately determined by the cost of injecting a charge unto the array from the source and the drain. At all α except for the values that lead to the minimum V_T for a given array length, the difference in the charge occupying the first and last islands, Q_1-Q_N, equals $N-1$. At the minimum values of V_T, this charge difference equals $N-2$.

The clean case of a related system was studied by Hu and O'Connell.[52] They analyzed a one-dimensional array of N

gated junctions with equal junction capacitances C_J and equal gate capacitances C_g. Due to the finite value of C_J charges in a given island interact with charges in other islands and with charges in the electrodes. With an applied bias voltage, the interaction between charges in the electrodes and in the islands results in a bias induced potential drop at the bulk junctions. Once a charge is injected unto the array, it will have no difficulty in traveling through it, and the threshold voltage equals the voltage required for injection of a charge from the electrodes. As the ratio C_g/C_J increases, the threshold voltage of a long array tends to an N-independent value of the order of the charging energy. The on-site case discussed here corresponds to $C_J=0$. If one extrapolates the case discussed by Hu and O'Connell[52] to $C_g/C_J \to 0$, an N-independent threshold voltage would be expected for onsite interactions. As shown above, the threshold voltage of clean arrays does not satisfy this prediction, as at zero temperature the charges cannot travel freely through the array, and the threshold voltage increases with the number of islands.

In the case of disordered arrays, V_T depends on the array configuration of disorder $\{\phi^{\mathrm{dis}}\}$. The threshold voltage depends on α, in a way similar to the clean case [see Fig. 1(b)]. As shown in Fig. 1(c), this dependence on α disappears in the average value and we recover the prediction of Middleton and Wingreen.[31] For the disordered case, Middleton and Wingreen[31] predicted a linear dependence of the threshold voltage on the array length. Only junctions with upward steps in the disorder potential $\Phi_i^{\mathrm{dis}} > 0$ prevent the flow of charge. The downward steps $\Phi_i^{\mathrm{dis}} < 0$ facilitate it. In average there are $N/2$ upward steps. To overcome such steps, a charge gradient has to be created in those junctions. For onsite interactions this results in $\langle V_T \rangle = E_c^{isl} N$.[67] As shown in the inset of Fig. 1(c), we also recover the relationship for the fluctuations in the threshold predicted by Middleton and Wingreen,[31] $\delta V_T \propto N^{1/2}$.

B. Flow of current

For bias voltages larger than threshold the current I can flow, but it is a strongly nonlinear function of voltage. The current depends on the charging energy and number of islands, on the presence or not of charge disorder in the array, on the resistances of the junctions, and on the asymmetry of the applied bias voltage.

1. Linear dependence close to threshold

There has been some controversy regarding the power law of the current with $(V-V_T)$ through one-dimensional disordered arrays for voltages close to V_T, $I \sim (V-V_T)^{\nu}$. Middleton and Wingreen[31] predicted linear behavior for both the long- and short-range interactions. Reichardt and Reichardt[57] found a square-root behavior using a model with a $1/r$ interaction between the charges in the islands. $\nu=1/2$ is the exponent corresponding to an sliding charge-density wave. They argued that the value $\nu=1$ obtained by Middleton and Wingreen[31] is a consequence of using voltages, which are not small enough. Kaplan *et al.*[35] found $\nu=1$ in the long-range limit of an array of dots capacitively coupled to their nearest neighbors. Jha and Middleton[56] argued that the dependence of the current of disordered arrays in the onsite limit on $(V-V_T)$ for voltages marginally greater than V_T is linear with an slope inversely proportional to the length of the array. In Fig. 2 we show that the current varies linearly with respect to $V-V_T$ for very small $V-V_T$ but that the slope is not inversely proportional to N.

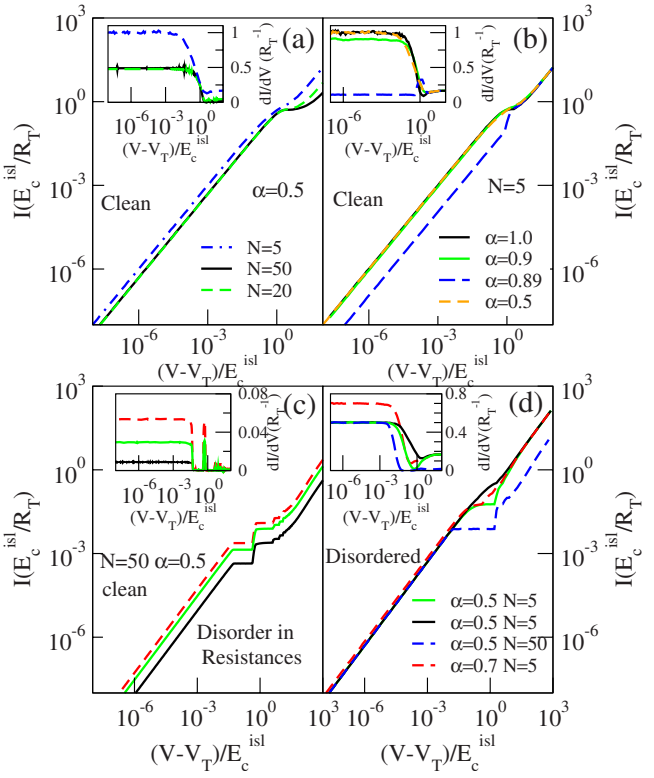

FIG. 2. (Color online) Main figures: I-V curves in logarithmic scales for different array parameters. The insets show the derivatives (in units of $1/R_T$) of the curves plotted in the main figures. The linear dependence of current on voltage (constancy of the derivative) is clearly seen in all the plots but it disappears for $V-V_T \sim 10^{-2} E_c^{isl}$, which for the cases shown corresponds to $(V-V_T)/V_T \sim 10^{-4}$. (a)–(c) show I-V curves corresponding to arrays without charge disorder. All junction resistances are equal in (a) and (b). As shown in (a) for clean arrays the slope of the linear dependence does not depend on the number of islands except for $\alpha=0.5$, which shows an even-odd effect with a slope equal to unity and 0.5 for odd and even number of particles, respectively. (b) The dependence of slope on α can be nonmonotonous if there is a change in the contact junction which acts as a bottle-neck. (c) I-V curves for arrays with junction resistances randomly assigned varying between $(5-11)R_T$ (upper curve), $(8-21)R_T$ (middle curve), and $(23-83)R_T$ (bottom curve). The different slopes are due to different resistances at the bottleneck junction. (d) I-V curves of disordered arrays with homogeneous contact resistance. The $\alpha=0.5, N=5$ curves correspond to different realizations of disorder. The even-odd effect present for $\alpha=0.5$ in the clean case has disappeared as just one contact junction acts as bottle-neck.

The current through the array is equal the average time necessary to transfer a charge through the array, which adds the time involved in all the processes in the sequence of tunneling events from the moment in which charge enters the

array from one electrode until it leaves the array to the other one. If the time associated to tunneling at a given junction is much larger than the time involved in the rest of processes, this junction acts as bottleneck and the time necessary to transverse the array is approximately equal to the time involved in the tunneling through this junction. On average this time is equal to the inverse of the tunneling rate given by Eq. (1). The current can be approximated by the tunneling rate across the bottleneck junction.

Charges can enter only through the contact junctions from the leads. Below threshold, but close to it, the tunneling at the contact junctions costs finite energy and transport is suppressed. This cost in energy is reduced by the applied bias voltage until at threshold it is zero at the entrance junction. With $V > V_T$ but very close to V_T, the entrance junction acts as bottleneck for transport. At zero temperature $\Gamma_T = -\Delta E/R$. If V_T is determined by the source junction,

$$I = \frac{1}{R_1}\alpha(V - V_T) \tag{16}$$

as ΔE for tunneling through this junction is $-\alpha(V-V_T)$. Analogously, if V_T is determined by the drain junction, $\Delta E = -(1-\alpha)(V-V_T)$ and

$$I = \frac{1}{R_{N+1}}(1 - \alpha)(V - V_T). \tag{17}$$

Both source and drain junctions have to be taken into account in the clean symmetrically biased case when N is odd.

$$I = \left(\frac{1}{R_1} + \frac{1}{R_{N+1}}\right)\frac{1}{2}(V - V_T). \tag{18}$$

For even N even and $\alpha = 0.5$ current flow requires that charge enters through both junctions and the current is approximately equal to

$$I = \frac{2}{R_1 + R_{N+1}}\frac{1}{2}(V - V_T). \tag{19}$$

The even-odd asymmetry in the slope has the same origin as the threshold voltage. This behavior is observed in Fig. 2. The linear behavior is clearly appreciated in both the log-log scale in which the main figures are plotted as well as in the constancy of the derivatives in the insets. The dependence of the slope of the I-V curves is better seen in dI/dV plotted in the insets. As seen in Fig. 2(a) dI/dV is equal for the $\alpha = 0.5$, $N=50$ and $N=20$ curves, i.e., independent on the array length. On the contrary, it is doubled for $N=5$ due to the even-odd alternancy predicted by Eqs. (18) and (19). The α dependence is studied in Fig. 2(b). From top to bottom, the change in slope with α is smooth and given by α/R_1, as predicted by Eq. (16), but turns nonmonotonously if currents starts being controlled by Eq. (17) with slope $(1-\alpha)/R_{N+1}$. As expected from the above discussion, the slope is affected by disorder in resistances in Fig. 2(c) but not by charge disorder in Fig. 2(d), except in the lose of the even-odd effect present in the clean case for $\alpha = 0.5$. So far, there are no experiments available in completely one-dimensional arrays, but there are a few in quasi-one-dimensional systems. The approximate power-law measured[51] at voltages $(V-V_T) \sim 0.01 V_T$ is larger than unity, which has been attributed to the fact that the system is not strictly one dimensional. The linear behavior in Fig. 2 appears for several orders in magnitude. In spite of this, it disappears for $V - V_T \approx 10^{-2}$ or $(V-V_T)/V_T \sim 10^{-4}$ (much smaller than the values at which the approximate power law have been measured). The magnitude of the current is probably too small for this linearity to be detected experimentally.

2. Intermediate regime

We have found that linearity gives rise to sublinear behavior when the time of the other tunneling processes become relevant compared to the time spent at the bottleneck. Upon increasing V the tunneling rates of the different processes involved in the transport become more homogeneous. To obtain sublinear behavior, it is just necessary that the two slowest processes in a sequence have comparable rates. The loss of linearity can depend on the resistance of the junctions when a nonbottleneck junction has a resistance much larger than the bottleneck one. The bottleneck character of the junction disappears faster for longer arrays as there are more tunneling processes, which will contribute to the total time. In the disordered case, the energy gain of some of the tunneling processes is smaller than in the clean case and the contact junctions can stop being the bottleneck earlier, i.e., for smaller $V-V_T$. However, in general we have not found very significative differences for different array parameters in the value of the bias voltage at which the linearity disappears.

The energy of a tunneling process through an inner junction does not depend on the applied voltage (except via the charge accumulated on it), so when a bulk junction controls the transport, the current is independent on voltage showing a characteristic staircase profile. The existence of the Coulomb staircase has been known for a long time.[23,61–63] Early claims reported a Coulomb staircase only in the asymmetrically biased case.[23] More recent results in clean capacitively coupled nanoparticle arrays show that a staircase also emerges in a symmetric array under symmetric bias[60] but claim that the I-V characteristic for an N-dot array under forward bias is identical to that for a $2N$-dot one under symmetric bias. We show here that while the appearance of the staircase is generic, the last statement is not correct.

The current has kinks at those voltages, which allow new transport processes, changing the maximum number of charges that can be accumulated at the first or last island. These voltage values depend on α and on the existence of charge disorder in the array but not on resistance disorder. To allow the addition of an extra charge in the first or last nanoparticle requires an increase in potential drop at the contact junction equal to $2E_c^{isl}$. In the clean case, when $\alpha = 1,0$ only one electrode changes its potential and the width of the steps in bias voltage is $2E_c^{isl}$. On the other hand, when $\alpha = 1/2$ the change in potential of a given electrode is just the half of the change in bias voltage and steps appear in intervals of $4E_c^{isl}$.

With charge disorder and $\alpha = 0,1$ the position of the kinks in voltage depends on the disorder configuration, but the width of the voltage intervals between the kinks does not change, as new charges are added through a single junction.

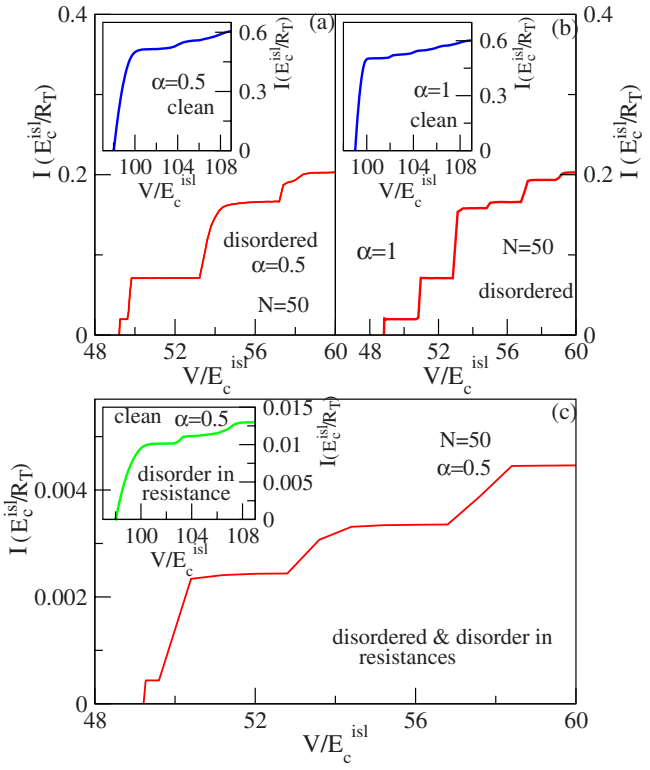

FIG. 3. (Color online) *I-V* curves for $N=50$ and different array parameters at intermediate bias voltages showing the Coulomb staircase. Insets in (a) and (b) correspond to an array without charge or resistance disorder and respectively $\alpha=0.5$ and $\alpha=1$. The current shows a big jump at threshold and very weak small steps at higher voltages. The width of the steps is $4E_c^{isl}$ in (a) and $2E_c^{isl}$ in (b). Main figures in (a) and (b) show *I-V* curves for arrays with charge disorder but homogeneous resistances. $\alpha=0.5$ in (a) and $\alpha=1$ in (b). The first step height is reduced and the staircase structure is more pronounced than in the clean case because tunneling processes in the bulk can have small energy gain and become the bottleneck more easily. The width of the steps in (b) remains equal to $2E_c^{isl}$ as in the clean case. In (a) there are two different step lengths which alternate and sum to $4E_c$, corresponding to the entrance of charge through both electrodes. The *I-V* curves in (c) correspond to arrays with resistance disorder and $\alpha=0.5$ without charge disorder in the inset, and with charge disorder in the main figure.

If $\alpha=1/2$, charges enter from both contact junctions but the corresponding kinks in the current do not appear at the same position. While the width of a kink corresponding to a given contact junction remains equal to $4E_c^{isl}$, in a general case in the *I-V* characteristic there will be two kinks in each $4E_c^{isl}$ interval in bias voltage due to the alternative position of the kinks of both contact junctions. Except in very special cases, the separation of kinks does not equal $2E_c^{isl}$. If the onsite interaction case discussed here can be experimentally reproduced, the width of the steps in the *I-V* curve can differentiate α values.

The position of the kinks in the clean and disorder cases can be observed in Fig. 3. Two main features can be observed. For clean arrays [insets in Figs. 3(a) and 3(b)] at the onset the current shows a big jump. Once the charge gradient is created and the charge can transverse the array, it flows easily. The steps at higher voltages are much smaller but have the width predicted above. In the main figures corresponding to disordered arrays, the large big jump has disappeared and steps are more clearly observed. Two step widths, which add $4E_c^{isl}$, are seen for $\alpha=0.5$ and just steps with width $2E_c^{isl}$ appear for $\alpha=1$.

Disorder in the resistances does not modify the voltages at which kinks in the current appear but it does affect the staircase profile. The staircase profile is modified in Fig. 3(c), compared to Fig. 3(a) due to the disorder in resistances. A very large resistance in a bulk junction can sharpen the steps, as it creates a bottleneck for the current at a junction with an associated energy for tunneling, which does not directly depend on bias voltage, but the opposite behavior can also take place if the large resistance if found at any of the contact junctions. The way in which the *I-V* curve is affected by disorder in resistance depends on the particular resistance and charge-disorder distributions.

3. Linear regime at high voltages

At very high voltages, the charge gradient ensures that all the tunneling processes to the right decrease the energy. The corresponding tunneling rates are $\Gamma_i=R_i^{-1}(\Phi_i-E_i^{e-h})$ and the total tunneling rate Γ^{tot} for no resistance disorder is $\Sigma_{i=1}^{N+1}\Gamma_i$. Having in mind that $\Sigma_{i=1}^{N+1}\Phi_i=V$, $\Gamma^{\text{tot}}=R_T^{-1}(V-\Sigma_{i=1}^{N+1}E_i^{e-h})$. This rate is independent of the selected tunneling process. To transfer a charge from the source to the drain requires in average $(N+1)$ tunneling events. The average current is

$$I_{\text{asympt}} \sim \frac{1}{(N+1)R_T}\left(V-\sum_{i=1}^{N+1}E_i^{e-h}\right). \tag{20}$$

A linear dependence is recovered. The asymptotic linear *I-V* does not extrapolate to zero current at zero voltage but it cuts the zero current axis at a finite offset voltage. The analytical prediction (20) is compared in Figs. 4(a) and 4(c) with numerical results. The slope of the current does not depend on α or the existence of charge disorder but only on the number of junctions $(N+1)$. The slope equals the sum of the resistances in series. Asymptotically this curve cuts the $I=0$ axis at the offset voltage $V_{\text{offset}}=\Sigma_{i=1}^{N+1}E_i^{e-h}$. This value is, in general, different from the threshold voltage and independent of the resistance of the junction and α.

Previous derivation is valid even if there is inhomogeneity in the value of island capacitances but relies on the homogeneity of the junction resistances through the array. If this is not the case the total tunneling rate of each step in a sequence is $\Gamma^{\text{tot}}=\Sigma_{i=1}^{N+1}R_i^{-1}(\Phi_i-E_i^{e-h})$. We assume that, on average, the charge gradient would be such that it ensures a uniform tunneling rate Γ^{uni} through all the junctions. The potential drop, which gives such a tunneling rate, is $\Phi_i=R_i\Gamma^{\text{uni}}+E_i^{e-h}$ and $\Gamma^{\text{uni}}=(V-\Sigma_{i=1}^{N+1}E_i^{e-h})/R_{\text{sum}}$ with $R_{\text{sum}}=\Sigma_{i=1}^{N+1}R_i$. There are $(N+1)$ possible tunneling events at each step in a sequence and $(N+1)$ steps. Both $(N+1)$ factors cancel out. The resulting average current is

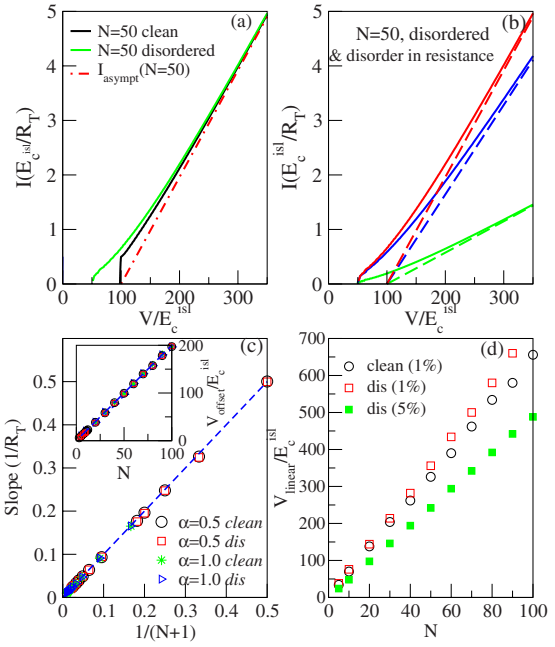

FIG. 4. (Color online) (a) *I-V* curves calculated up to high voltages for $N=50, \alpha=0.5$ for clean and charge-disordered arrays. Both curves approach the same asymptotic curve at high voltages, even if the threshold voltage is quite different. Theoretical prediction is included for comparison. (b) Computed *I-V* curves for charge-disordered arrays with different junction resistances (solid lines) with their theoretical asymptotic predictions (dashed lines). From top to bottom, a curve corresponding to an array with all-equal junction resistances, an array with randomly assigned resistances, and an array with all-equal random resistances, except the first one which is ten times R_T. The slope differs but all the curves have equal offset voltage. (c) Slope (main figure) and offset voltage (inset), which give better fitting to the numerically computed current at high-voltages as a function of the number of islands in the array for several array parameters, all of them with homogeneous junction resistances. For comparison the theoretical prediction (dashed-line) is included. The offset voltage equals $\Sigma_{i=1}^{N+1} E_i^{e-h}$, and the slope is inversely proportional to the sum of the junction resistances added in series. Independence on the value of α and the presence or absence of charge disorder is observed. (d) Voltage at which the high-voltage asymptotic behavior is reached, estimated as the value at which $I-I_{\text{asympt}}/I$ is smaller than a given value, 1% and 5% in the figures. It is slightly larger for disordered arrays, it increases linearly with the number of islands, and it is approximately 3 and 2.5 times the offset voltage.

$$I_{\text{asympt}} \sim \frac{1}{R_{\text{sum}}}\left(V - \sum_{i=1}^{N+1} E_i^{e-h}\right). \tag{21}$$

The slope in the current corresponds to the addition in series of all the resistances. This equation reduces to Eq. (20) when all resistances are equal. The predicted asymptotic high-voltage behavior is observed in Fig. 4 for arrays with different parameters. Good agreement with Eq. (21) justifies the uniform tunneling rate assumption. The voltage V_{linear} at which the linear behavior is reached is estimated in Fig. 4(d). As longer is the array larger voltages have to be applied to reach V_{linear}. It is approximately three times the offset voltage and slightly larger in the presence of charge disorder. In long arrays V_{linear} can become very large and the linear behavior will not be easily reached experimentally.

C. Potential drop through the array

The potential through the array can nowadays be measured,[66] but to our knowledge, it has not been studied theoretically. In conventional Ohmic systems with a linear current-voltage relation $V=IR$, the potential drops homogeneously through the array if the resistivity of the system is homogeneous. When the proportionality constant between voltage and current is given by the sum of the resistances in series, but these resistances are not all equal, the voltage drop at each point is proportional to the local resistance. The nanoparticle array *I-V* characteristics are highly nonlinear and in general it is not obvious how the potential drops through it. At the islands the potential is the sum of the disorder and charge terms, while at the electrodes the potential is controlled by the applied bias. In this section we study the potential drop through the array at low, intermediate, and high voltages and show that in none of these regimes the potential drop at a given junction is strictly proportional to its resistance.

1. High-voltage regime

We start with the high-voltage linear regime, as it is the easiest to understand. Figure 5 shows the average potential drop in a clean and a disordered array for a given bias voltage in the high-voltage linear regime. All the junction resistances are equal in the top figures. The average voltage drop is equal in both the clean and disordered case, and at first sight it seems linear. A linear potential drop through the array implies a homogeneous average junction potential drop $\bar{\Phi}_i$. However, at the contact junctions, $\bar{\Phi}_i$ is approximately E_c^{isl} times smaller than at the bulk junctions. The voltage drop at each junction is not equal to the current divided by the junction resistance either, as could be naively expected. The origin of this effect is the different values of the excitonic energy (3).

At high voltages the *I-V* curve is linear but the total voltage drop through the array does not equal $R_{\text{sum}}I$ due to the offset voltage $V_{\text{offset}}=\Sigma_{i=1}^{N+1} E_i^{e-h}$. The excitonic energy E_i^{e-h} is $2E_c^{isl}$ at the bulk junctions and approximately E_c^{isl} at the contact ones. Only the extra potential drop $\bar{\Phi}_i - E_i^{e-h}$ at each junction gives a finite contribution to current through it. On average,

$$I = \frac{1}{R_{\text{sum}}}(\bar{\Phi}_i - E_i^{e-h}). \tag{22}$$

From current conservation at high voltages, the average potential drop through the array

$$\bar{\Phi}_i = E_i^{e-h} + \frac{R_i}{R_{\text{sum}}}(V - V_{\text{offset}}). \tag{23}$$

It is not affected by the presence of charge disorder in the array (but it would change if capacitances are not homoge-

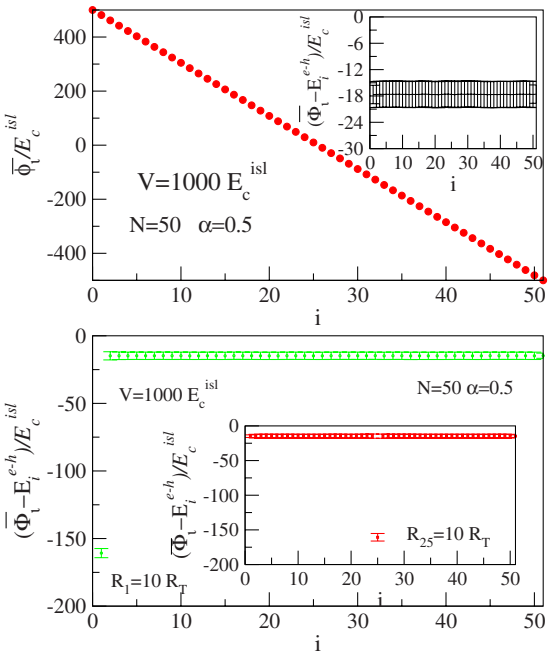

FIG. 5. (Color online) Top: main figure shows the average potential at the islands $\bar{\phi}_i$ as a function of position for a disordered array with $N=50$, $\alpha=0.5$, and all junction resistances equal. As shown in the inset the average potential drop at the junctions $\bar{\Phi}_i$ is homogeneous only once the excitonic energy is subtracted. The value subtracted is smaller at the contact junctions where $\bar{\Phi}$ is smaller. The error bars give an estimation of the fluctuations of the potential drop. Bottom: main figure (inset) show the average potential drop, with error bars giving its root mean square at the junctions with the excitonic energy subtracted corresponding to a clean array with the first (middle) junction ten times larger than the rest. $\bar{\Phi}_i - E_i^{e-h}$ is proportional to the junction resistance. This proportionality holds only once the excitonic energy is subtracted.

neous via E_i^{e-h}). As observed in Fig. 5, Eq. (23) gives a good estimate of the potential drop. The validity of Eq. (23) is better seen when $\bar{\Phi}_i - E^{e-h}$ is plotted. It is proportional to the resistance of the junction and equal in every junction if all resistances are the same. This statement is valid independently of the position of the resistance, as shown in the bottom figure of Fig. 5 and its inset and on the asymmetry α of the applied voltage (not shown). The dependence of $\bar{\Phi}_i$ on the junction resistance is easily understood. The tunneling probability through a junction is inversely proportional to its resistance. When the resistance is very large, the charge has a lesser tendency to jump from an island to its neighbor and it will spend more time in the island producing a dependence of the time-averaged potential drop on the junction resistance distribution.

As seen above, in this high-voltage linear regime the current can be obtained from the average tunneling rate and correspondingly from the average potential drop. Deviations of the average value $\delta\Phi_i$, i.e., the root mean square (rms), are shown in the inset in Fig. 5 in the form of error bars. They are slightly smaller at the contact junctions as the potential at the electrodes is restored to its nominal value via a battery prior to any tunneling event and larger at junctions with a larger resistance. Fluctuations in the local voltage drop Φ_i increase with applied bias voltage as the number of possible charge states and the width of the distribution of hopping energies do. Fluctuations are larger at those junctions with a larger resistance but $\delta\Phi_i/\bar{\Phi}_i$ is smaller.

2. Low-voltage regime

Close to threshold the current depends linearly on $V-V_T$. The average potential drop mainly reflects the charge state of the array at threshold. This charge state depends on the asymmetry of the voltage drop α and disorder and in a symmetrically biased clean array on the even or odd number of islands. For $\alpha=1$, charges enter from the source and $(N-1)$ bulk junctions prevent charge motion. If an electron reaches the last nanoparticle, it can freely jump onto the drain at zero potential. There is no charge gradient at the drain junction. Consequently, the potential drop at this junction vanishes at threshold. On the contrary, at the $(N-1)$ bulk junctions there is a charge gradient equal to unity, with the corresponding potential drop $2E_c^{isl}$. To allow current $V_0-\phi_1$ equals the excitonic energy of the first junction, approximately equal to E_c^{isl}. Close to threshold, as the bottleneck for the current is the entrance of electrons from the source the charge state of the array is most of the time equal to the one at threshold and only perturbed by the fast passage of charges. The average potential drop, plotted in Fig. 6(a) for a clean array with all junction resistances equal, is almost the same as the static potential drop at threshold.

For $\alpha=1/2$ and odd number of particles, at threshold the charge gradient and charge potential drop in a clean array are, respectively, one and $2E_c^{isl}$ at the bulk junctions. At the contact junctions the potential drop is E_c^{isl}. As in the $\alpha=1$ case discussed above, the average potential drop in the linear regime close to threshold is very close to the one found at threshold, which equals the excitonic energy at each junction, $\bar{\Phi}_i - E_i^{e-h} \sim 0$, what can be seen in the main figure in Fig. 6(b). When the number of particles is even, the charge gradient at one of the junctions vanishes. As shown in the inset of Fig. 6(b), $\bar{\Phi}_i - E_i^{e-h}$ in the bottleneck regime is positive and equal for all the junctions. This reflects that every junction is uncharged with equal probability. In the disordered case, only those junctions with upward steps in the disorder potential are charged, and this is reflected in the average potential drop, in Fig. 6(c) which adds disorder, charge, and bias potential. It fluctuates between $-2E_c^{isl}$ and 0, instead between $-E_c^{isl}$ and E_c^{isl} as the disorder potential does.

The threshold voltage does not depend on the resistance of the junctions, but the flow of charge does. This appears on the average potential drop on such a small scale that even if the threshold voltage potential drop is subtracted at each junction and for reasonably large changes in resistance it is not visible [see main figure in Fig. 6(d)]. This differs from the dependence observed in the high-voltage regime. For extremely large values of the resistance disorder, a weak effect on the average voltage at bias close to threshold can be seen (not shown). In this case, the potential drop at a junction with a larger resistance is slightly larger than at the rest. At the adjacent junctions, it is slightly smaller, which reflects the

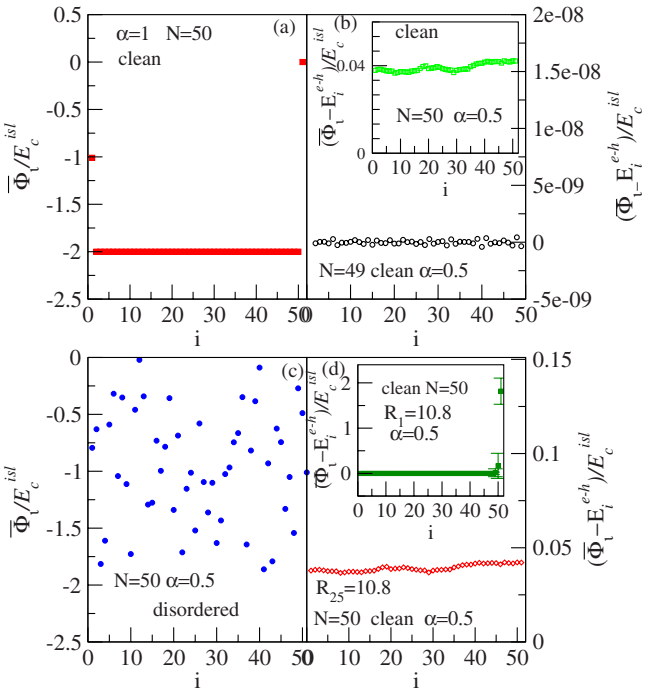

FIG. 6. (Color online) Average potential drop through the array at bias voltages very close to threshold. Fluctuations are smaller than the symbols. (a) Clean $N=50$ array with $\alpha=1$. The potential drop vanishes at the last junction, as the source is at zero potential and there is no charge gradient at this junction. At the first junction is equal to the excitonic energy, which at a contact junction is approximately E_c^{isl}. (b) Average potential drop for a symmetrically biased $N=49$ array in main figure ($N=50$ in the inset) with the excitonic energy subtracted. Once the excitonic energy, associated to the charge gradient at threshold has been subtracted the average potential drop almost vanishes for $N=49$. The homogeneous and positive value for $N=50$ reflects that every junction is uncharged with equal probability. (c) Average potential drop at the junctions $\bar{\Phi}_i$ corresponding to a disordered array with $N=50$ islands and $\alpha=1/2$. (d) Main figure (inset): $\bar{\Phi}-E^{e-h}$ corresponding to a $N=50$ clean array with the middle (first) junction resistance 10.8 larger than the other ones.

average charge state of the nanoparticles joined by the large resistance. A special case is a N-even clean $\alpha=0.5$ array with the first resistance larger than the other ones, shown in the inset in Fig. 6(d). The average potential drop differs considerably with respect to the one found in the inset in Fig. 6(b). The presence of the larger resistance at a contact junction modifies the average charging of the array and selects the opposite contact junction as the one which lacks charge gradient.

The rms of the junction potential drop at low bias voltages are very small in some of the cases analyzed, of order of $10^{-3}E_c^{isl}$ in the main figures in Figs. 6(a) and 6(b). The error bars are small because most of the time the array is at the threshold charge state. This is not the case in the inset in Fig. 6(b) where fluctuations are or the order of $0.3E_c^{isl}$, or in the inset in Fig. 6(d) where they are small everywhere except at the last two junctions where they are of order E_c^{isl}. Disorder also increases the fluctuations in the average voltages to values of the order of the charging energy.

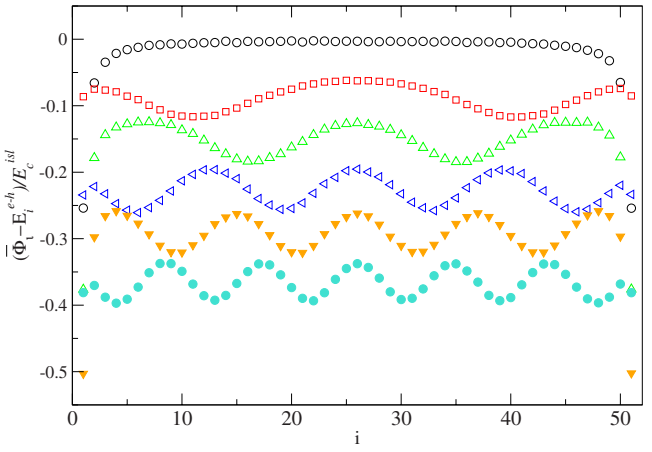

FIG. 7. (Color online) Average potential drop, with the excitonic energy subtracted $\bar{\Phi}_i-E_i^{e-h}$ at the junctions as a function of position at several values of the bias voltage, for which the current is in the Coulomb staircase regime, corresponding to a clean $N=50$ array and $\alpha=1/2$. From top to bottom $V=102,104,106,108,110,112E_c^{isl}$. Curves have been vertically displaced to avoid overlap. The potential drop show almost regular oscillations which reflect a stationary (but not static) charge ordering. The number of maxima and minima does not change within a step and increases in two (for $\alpha=1/2$) from one steps to the next one. The position of maxima is slightly adjusted within a step. They start appearing close to the electrodes and reflect the entrance of charge from them.

3. Intermediate voltage regime

The most interesting regime to analyze the voltage drop is at intermediate voltages where the I-V curve show the Coulomb staircase. For the case of a clean array with capacitively coupled nanoparticles, Stopa[60] argued that the steps in the I-V characteristic correspond to alternation of the charge density between distinct Wigner crystalline phases. The possibility of a state with charges periodically ordered to minimize their repulsion, if present, should lead to oscillations in the potential drop along the array. Such an observation would be a clear evidence of correlated motion.

The average potential drop (with the excitonic energy subtracted) through the array for several voltages corresponding to clean $N=50$ nanoparticle arrays is shown in Fig. 7. Clear oscillations are seen. The number of maxima and/or minima in the potential drop does not change in a given step in the Coulomb staircase. For symmetrically biased arrays, they increase in pairs from a step to the next one. For odd and/or even number of particles, there is always a minimum and/or maximum at the center of the array. The other maxima and minima tend to be as equally spaced as possible. Incommensurability between the period of the oscillations and the lattice can distort equal displacement. When new maxima or minima appear, they are closer to the source and drain electrodes and move inward, producing a movement of the other maxima and minima, with increasing voltage. This can be taken as a finite-size effect of the crystal state. As the number of charges in the array increases with increasing bias voltage, the amplitude and period of the oscillations decreases, approaching the high-voltage regime for which $\bar{\Phi}_i-E_i^{e-h}$ is homogeneous.

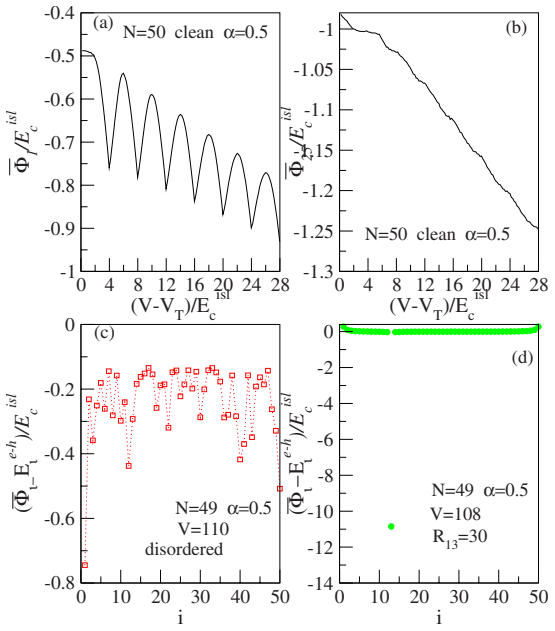

FIG. 8. (Color online) (a) and (b) show the average potential drop at the first and 25th junctions as a function of bias voltage for a clean array with $N=50$ islands, $\alpha=1/2$, and no resistance disorder at intermediate voltages. The average potential drop at the contact junction oscillates as a function of the bias. The potential drop at the center of the array depends monotonously on V. (c) and (d) show $\Phi_i - E_i^{e-h}$ for charge and resistance disordered 49-island arrays, respectively, and $\alpha=1/2$. The Coulomb staircase is much more pronounced in the presence of disorder. However, as shown here, the oscillatory potential drop structure found in Fig. 7 and characteristic of crystal like physics is destroyed.

For $\alpha=0,1$ the step width is the half compared to $\alpha=1/2$. Charges enter through just one of the contact junctions. The different in number of maxima and/or minima between two adjacent steps is one (not shown) and the potential drop at the central junction alternates between being a maximum and a minimum. The even-odd effect disappears.

The anomalous potential drop can be also seen in the potential drop at a given junction as a function of the bias voltage, shown in Figs. 8(a) and 8(b) for junctions 1 and 25 for a clean symmetrically biased 50-islands array. At the first junction the potential drop show clear oscillations as a function of the bias voltage, which reflect that new charges state at the first island are allowed. The potential drop increases until an extra charge can be accumulated at the first nanoparticle; for larger voltages the average occupation of first island increases and the voltage decreases smoothly until a new value at which it increases again as the increase in occupation of first island cannot compensate the increase in the electrode potential. Oscillations, but less regular and less pronounced due to the movement of maxima and minima discussed above, are also observed at intermediate junctions. The potential drop is much more homogeneous at the middle of the array, where there is always a minimum (or a maximum) in the potential drop.

Charge or resistance disorder alters the charge motion and frustrates the formation of this crystal-like state, as seen in Figs. 8(c) and 8(d). This is the opposite behavior that would be naively expected if one just associates the appearance of plateaus with the oscillations in voltage drop and emphasizes that the step profile is just a consequence of the dependence on the bias voltage of the tunneling rate of the processes, which control the current. The rms of the junction potential drop (not shown) is larger than at low voltages and smaller than at high voltages. It is of the order of the excitonic energy and reflects the variation in occupation of the island. It slowly increases with voltage.

IV. LONG-RANGE INTERACTIONS: SCREENING AND CORRELATIONS

A. Interaction potential of an array of spheres

In Sec. III we assumed that the charges in different conductors did not interact. In free space two pointlike charges interact via Coulomb law with an $1/r$ dependence, being r the distance between them. The same dependence applies for charges in two conductors if they are far apart. When two conductors become closer together the mobile charges in their surfaces screen the interaction between the charges in them, which then differs from the $1/r$ Coulomb law. Other metallic systems in the surrounding environment contribute also to this screening. Here we describe the resulting interaction $C^{-1}_{\alpha\beta}$, measured in units of C^{-1}_{isl} and calculated as described in the Appendix.

In Fig. 9(a) we show how C^{-1}_{ii} and $C^{-1}_{i,i+1}$ and the excitonic energy E_i^{e-h} depend on the distance between the particles d/r^{isl} for the case of an array with $N=100$ equal-sized islands at the center of the array. The effects of screening start to be relevant for $d/r^{isl}<1-2$. At this value C^{-1}_{ii} deviates from unity and when $d/r^{isl}\to 0$, approximately at $d/r^{isl}=0.002$ it saturates at about 0.68. $C^{-1}_{i,i+1}$ increases following a $1/r$ law as d/r is reduced until $d/r^{isl}\sim 1-2$. Then it deviates from this law and finally it saturates at about $d/r^{isl}=0.1$. For large d/r^{isl}, E_i^{e-h} decreases when d/r^{isl} is reduced following the $1/r$ increase in $C^{-1}_{i,i+1}$. For $d/r^{isl}<2$, its value is affected both by the increase in $C^{-1}_{i,i+1}$ and by the decrease in C^{-1}_{ii} and at small distance is controlled by this last effect. Finally it saturates.

The dependence of $C^{-1}_{i,i+j}$ on j that we have obtained for the experimentally relevant case of an array of spherical particles is plotted in Fig. 9(b). Compared with a $1/r$ law, at short distance the screened interaction potential decreases and at large distances it increases. When the particles are very close, there is a bump in the renormalized interaction. The potential approaches the $1/r$ law from above. Only when two charges are in the same particle or at the nearest-neighbor one the interaction between them decreases. Some discussion on the origin of this bump is given in the Appendix.

Compared to other one-dimensional array geometries previously studied, in the case of spherical nanoparticles studied here, screening is less important than in the case of cubic islands[69] but larger than for the thin disks.[70] For the case of thin circular disks (with disk axis perpendicular to the array axis), Whan *et al.*[70] found that a $1/r$ law describes well the dependence of the nondiagonal inverse capacitance matrix elements on distance and that the diagonal elements are re-

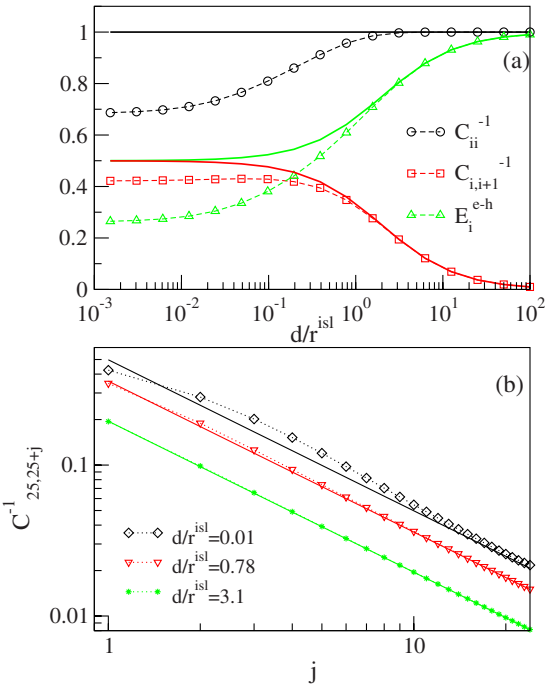

FIG. 9. (Color online) (a) Island inverse capacitance C_{ii}^{-1}, nearest-neighbor interaction $C_{i,i+1}^{-1}$, and excitonic energy, all in units of $(C^{isl})^{-1}$, at the center of a 50 nanoparticle array (without electrodes) as a function of the interisland separation. The solid lines give the value obtained with a $1/r$ interaction between charges. The effect of screening is evident for $d/r^{isl} \leq 1-2$. All the plotted quantities saturate to a finite value as d/r^{isl} vanishes. (b) Decay of the interaction potential from the center of a 50 nanoparticle array (without electrodes) as a function of island position for different values of d/r^{isl}. Inverse capacitances are given in units of $(C^{isl})^{-1}$. The solid lines correspond to an unscreened $1/r$ law. For large distances the $1/r$ law is approached from above. The bump is clearly observed only for very small d/r^{isl}. The effect of screening is negligible for $d/r \sim 3$. In (a) and (b) the dashed and dotted lines are included as a guide to the eye.

duced. On the other hand, Likharev and Matsuoka[69] analyzed the cases of an array of cubic islands and a continuum model in which the discrete periodic structure is replaced by a continuous dielectric medium. They found that the interaction potential could by approximated by the expression

$$U(m) = \frac{e^2}{a}\left(\frac{\alpha}{m_0}\exp\left(\frac{-\kappa m}{m_0}\right) + \frac{1}{m}\left[1 - \exp\left(\frac{-\kappa m}{m_0}\right)\right]\right). \tag{24}$$

In this expression, m is the distance in units of the array period a, $m_0 = r_0/a$, with $r_0 = S\epsilon/\pi$ as a characteristic decay length of the interaction. ϵ is the interisland dielectric constant, S is the junction surface, and κ is a fitting parameter with value very close to 1 and related to α by

$$\alpha = \frac{2}{\kappa} - \frac{\kappa}{2}. \tag{25}$$

Equation (24) shows a bump in the $1/r$ dependence similar to ours. We have tried to fit our results with Eq. (24) but have not been able.

The interaction that we have obtained differs considerably from the one resulting from capacitive coupling only to nearest neighbors, which has been extensively used in the literature. In such a model only $C_{ii} = C_0 + 2C$ and $C_{i,i\pm1} = -C$ are finite. For an infinite array its inverse

$$C_{ij}^{-1} = \frac{1}{C^{\infty}} e^{-|i-j|/\xi}, \tag{26}$$

with $C^{\infty} = 2Csh(\xi^{-1}) = (C_0^2 + 4CC_0)^{1/2}$. ξ increases with C/C_0 and can be viewed as the decay length of the interaction. Interactions on the same island are given by $C_{ii}^{-1} = 1/C^{\infty}$. In an array of finite length N, this value is approached, from below, as N increases. The onsite case is recovered when $C = 0$ and long-range interactions appear in the opposite limit $C_0/C \to 0$. In the later limit the interaction potential decays linearly with distance

$$C_{ij}^{-1} = \frac{1}{2C}\left(\frac{N}{2} - |i-j|\right). \tag{27}$$

The energy to create an electron-hole pair $E_i^{e-h} = 1/2C_{ii}^{-1} + 1/2C_{i\pm1,i\pm1}^{-1} - C_{i,i\pm1}^{-1}$ remains bound and equal to $1/(2C)$. On the contrary, the diagonal element $C_{ii}^{-1} = \frac{1}{4C}N$ diverges with the array size. There is not such a divergence in C_{ii}^{-1} with the array size in our model. C_{ii}^{-1} is finite as shown in Fig. 9(a).

To analyze the transport properties the array is sandwiched between two electrodes, much larger than each of the nanoparticles. To this end we consider a one-dimensional array of N nanoparticles placed in between two large spheres, with radius R, which play the role of the leads. The large size ensures large screening and that C_{00}^{-1} and $C_{N+1,N+1}^{-1}$ are much smaller than the islands C_{ii}^{-1}. The spherical shape greatly simplifies the calculations of the inverse capacitance matrix. For the size of the electrodes used in the text, $R \sim 50-100r^{isl}$, the inverse capacitance of the islands close to the electrodes is slightly reduced compared to those at the center, except for very small d/r^{isl}. For small d/r^{isl} the inverse capacitance of islands at the center of the array is almost insensitive to the presence of the electrodes. If the electrodes are much larger the dependence of the inverse capacitance matrix elements with the size of the electrodes can become nonmonotonous. This behavior, like the one found for small d/r^{isl} is probably associated to the spherical shape chosen to model the electrodes.

The interaction between the charges at the islands and those at the electrodes and the inverse capacitance elements of the electrodes determine λ_i^{α} and Λ_i^{α}, which control the polarization voltage drop through the array and to a large extent the current flow at small voltages. From Eq. (7) we see that λ_i^{α} depends both on the geometry of the electrodes and the array and on α. For most capacitance matrices, in particular, for the capacitance matrices discussed here, the polarization potential is not linear in the island label i and the potential drops are larger at the junctions close to the biasing leads. A linear drop of the polarization potential $\phi_i^{pol} = (\alpha - \frac{i}{N+1})V$, requires $\Lambda_i^{\alpha} = 1/(N+1)$ for all junctions and independence on α. In the onsite case, $\Lambda_i^{\alpha\{onsite\}}$ is finite only at junctions 1 and $N+1$ and given by $\Lambda_1^{\alpha\{onsite\}} = \alpha$ and

$\Lambda_{N+1}^{\alpha\{\text{onsite}\}}=\alpha-1$. In general, as the range of the interactions between charges increases, Λ_i^α is more homogeneous

In previous models[31] C^{-1} had dimension $N\times N$, including only the nanoparticles. The inverse self-capacitances of the electrodes, C_{00}^{-1} and $C_{N+1,N+1}^{-1}$, the inverse mutual capacitances between them, $C_{0,N+1}^{-1}=C_{N+1,0}^{-1}$, and the indirect term in Eq. (11) were neglected. In our model dimension of C^{-1} is $(N+2)\times(N+2)$. For the large electrodes used here $C_{K,L}^{-1}$ are small quantities, which do not influence the transport. On the other hand, the matrix element between the electrodes and the islands $C_{K,j}^{-1}$ appear in the definition of the polarization potential that plays an important role in the discussion of the transport. An expression for ϕ_{pol} analogous to Eq. (6) can be defined in previous models. For example, in the model used by Middleton and Wingreen,[31] the interaction between an island and an electrode is given by the interaction of the charge of the island with charges induced by the electrode in the islands immediately adjacent to the electrode. This interaction results in a polarization potential,

$$\lambda_i^{MW,\alpha}=C_{i-el}(\alpha C_{1i}^{-1}-(\alpha-1)C_{Ni}^{-1}). \tag{28}$$

Here C_{i-el} is the capacitance between the source or drain electrode and its adjacent island. In this model, except in the extreme long-range case $C_0/C\to 0$, the polarization potential does not decay linearly with distance and depends on the asymmetry of the bias potential. Other authors, within different models, have imposed a uniform polarization drop through the array.[57]

B. Screening of disorder potential

If interactions between the charges are short range, $(C_{ij}^{-1}=\delta_{ij})$, the set of disorder potentials $\{\phi_i^{\text{dis}}\}$, once the screening of the potential due to the mobile charges is taken into account, is uniformly distributed in the interval $-E_c^{isl}\le\phi_i^{\text{dis}}\le E_c^{isl}$. The probability associated with each pair, $(\phi_i^{\text{dis}},\phi_{i-1}^{\text{dis}})$, is a constant (see Fig. 10) and the distribution of the probabilities of the potential drops due to disorder across the array junctions, $\Phi_i^{\text{dis}}=\phi_i^{\text{dis}}-\phi_{i-1}^{\text{dis}}$, has the form[45]

$$P(\Phi^{\text{dis}})=\frac{1}{\Phi_{\text{MAX}}^{\text{dis}}}\left(1-\frac{|\Phi^{\text{dis}}|}{\Phi_{\text{MAX}}^{\text{dis}}}\right) \tag{29}$$

and $\Phi_{\text{MAX}}^{\text{dis}}=2E_c^{isl}$. In the presence of long-range interactions, the charges, which flow to compensate the large fluctuations of the disorder potential, modify potential at neighboring islands and the screened disorder is correlated.[45] The probability of each pair $(\phi_i^{\text{dis}},\phi_{i-1}^{\text{dis}})$ is no longer a constant. $P(\Phi^{\text{dis}})$ depends on the inverse capacitance matrix C^{-1}. To analyze these correlations and obtain the proper disorder potential distribution, we assign the potentials by first randomly assigning potentials to the islands $\phi_i^{\text{dis-bare}}$ in the interval $-W\le\phi_i^{\text{dis-bare}}\le W$ with W larger than the charging energy. We then find the equilibrium configuration of charges $\{Q_j^{\text{sc}}\}$ that occupy the array with island disorder potentials $\{\phi_i^{\text{dis-bare}}\}$ and grounded leads $(V_0=V_{N+1}=0)$ and redefine the potentials at each site using the expression

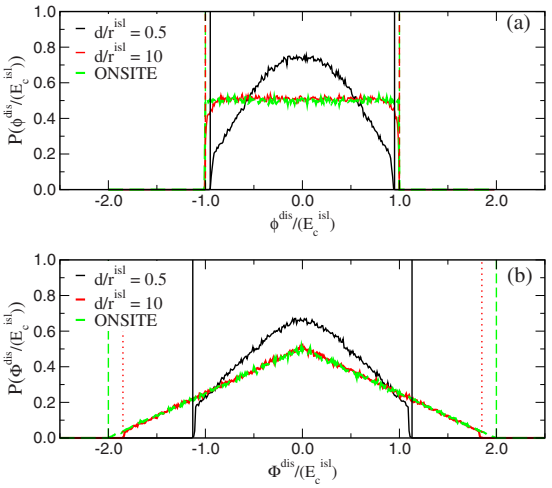

FIG. 10. (Color online) Probability distributions of disorder potentials ϕ^{dis} in (a) and disorder potential differences Φ^{dis} in (b) for 50 island in between two grounded leads with purely onsite interactions and with long-range interactions at two spacings: $d/r^{isl}=0.5$ and 10. The onsite Φ^{dis} distribution is described by Eq. (29) with $\Delta\phi_{\text{MAX}}^{\text{dis}}=E_{i,i-1}^{e-h,\text{onsite}}=2E_c^{isl}$, where $E_c^{isl}=1/(2C^{isl})$. For all the cases, $P(\phi^{\text{dis}})$ $[P(\Phi^{\text{dis}})]$ is finite valued for ϕ^{dis} (Φ^{dis}) between $\pm 0.5C_{ii}^{-1}$ $(\pm E_i^{e-h})$, which decreases with decreasing spacing. As the spacing decreases, the probability of having Φ^{dis} and ϕ^{dis} values close to zero increases. The vertical lines are included as guidelines to emphasize the edges of the distributions. The histograms average the values of the potentials of all islands and the values of the potential drops between all adjacent islands over many realizations of disorder $[O(>10^4)]$.

$$\phi_i^{\text{dis}}=\sum_{j=1}^{N}\tilde{C}_{ij}^{-1}Q_j^{\text{sc}}+\phi_i^{\text{dis-bare}}. \tag{30}$$

The effect of the screening charges $\{Q_j^{\text{sc}}\}$ is included in the redefined potentials $\{\phi_i^{\text{dis}}\}$ so we then reset the number of charges at each site to zero to avoid double counting the charge when we calculate the total electrostatic energy of our system.

Following the redefinition of the disorder potentials, we find that on average the distribution of the disorder potentials and the disorder potential drops $\{\Phi_i^{\text{dis}}\}$ between adjacent islands are independent of W.

The values of $\{\phi_i^{\text{dis}}\}$ and $\{\Phi_i^{\text{dis}}\}$ are bound by $\pm C_{ii}^{-1}/2$ and $\pm E_i^{e-h}$, respectively. When in this state, adding an additional charge to any island in the array increases the energy of the system. The energy of adding an additional charge to an island from a large electrode outside the system with negligible self-inverse capacitance is given by $E_i^{\text{add}}=(1/2)C_{ii}^{-1}\pm\phi_i^{\text{dis}}$, where the top (bottom) sign refers to the change in energy of the system as a result of adding a positive (negative) charge to island i. Since $E_i^{\text{add}}>0$ when the array is in equilibrium, the disorder potential values $\{\phi_i^{\text{dis}}\}$ must lie between $\pm(1/2)C_{ii}^{-1}$. Additionally when the array is in equilibrium state, the energy to hop between all pairs of adjacent sites must be greater than zero. From Eq. (3), the disorder potential differences Φ_i^{dis} are restricted between $\pm E_i^{e-h}$.

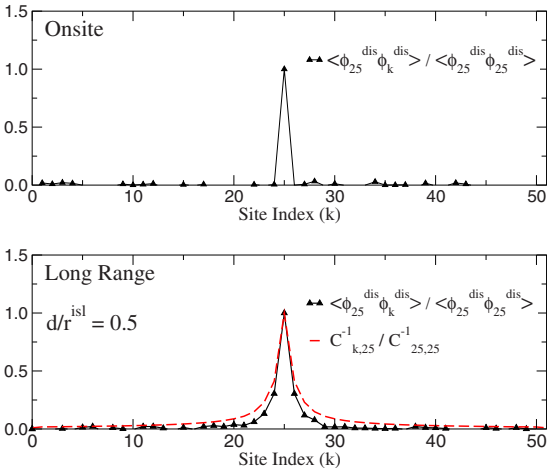

FIG. 11. (Color online) Comparison of $\langle \phi_{25}^{\rm dis} \phi_k^{\rm dis} \rangle$ normalized by $|\phi_{25}^{\rm dis}|^2$ for 50-island arrays with onsite (top plot) versus long-range (bottom plot) Coulomb interactions. In the presence of long-range interactions between the charges, the values of the disordered potentials are also correlated. $C_{k,25}^{-1}$ normalized by $C_{25,25}^{-1}$ is included in the long-range case to show that correlations in the disorder potentials are related to, but decay faster than the C^{-1} elements.

Figures 10(a) and 10(b) compare $P(\phi_i^{\rm dis})$ and $P(\Phi_i^{\rm dis})$ for arrays with purely on-site interactions ($C_{i\neq j}^{-1}=0$) with arrays with long-range interactions ($C_{i\neq j}^{-1}\neq 0$) at two spacings, $d/r^{isl}=0.5$ and $d/r^{isl}=10$. In Fig. 10(a), $P(\phi_i^{\rm dis})$ is a constant between $\pm E_c^{isl}$ for the on-site case. As the range of interactions increases (decreasing d/r^{isl}), the width of $P(\phi_i^{\rm dis})$ decreases because the disorder potential values are bound by $\pm 0.5 C_{ii}^{-1}$. Increasing Coulomb interactions also increases (decreases) the probability of small (large) values of $|\phi_i^{\rm dis}|$. In Fig. 10(b), the on-site $P(\Phi_i^{\rm dis})$ distribution is given by Eq. (29). Similar to the trends in Fig. 10(a), as the range of Coulomb interactions increases, the width of the distribution decreases and the probability of small (large) $|\Phi_i^{\rm dis}|$ values increases (decreases). The increased probabilities of small $|\Phi_i^{\rm dis}|$ are due to Coulomb correlations that make it more likely for the disorder potentials of neighboring islands to have similar values (see Fig. 11). Increasing the range of Coulomb interactions leads to a greater relative reduction in the width of $P(\Phi_i^{\rm dis})$ than $P(\phi_i^{\rm dis})$ because the former are bound by $\pm E_i^{e-h}$, whereas the latter are bound by $\pm 0.5 C_{ii}^{-1}$. In the onsite case, E_i^{e-h} equals $2E_c^{isl}$ for all junctions between two islands and increasing Coulomb interactions can reduce E_i^{e-h} significantly due to an decrease (increase) in C_{ii}^{-1} ($C_{i,i\pm 1}^{-1}$) [see Eq. (4)].

Our results for $P(\Phi_i^{\rm dis})$ differ to some extent from those by Elteto and co-workers,[45] calculated with an inverse capacitance matrix C_{ij}^{-1} that is finite only for nearest neighbors and charge disorder modeled by a set of stationary quenched charges. The distributions of Elteto and co-workers[45] are bound by $\pm C_{ii}^{-1}$ instead of E_i^{e-h} due to the lack of correlations in their quenched disorder model. We permit the interactions among the screening charges to determine whether or not the disorder potentials are correlated.

In Fig. 11, we plot $\langle \phi_i^{\rm dis} \phi_k^{\rm dis} \rangle$ to show how interactions among charges affect the correlations among disorder potentials. In the onsite case, correlations are finite only if $i=j$. In this case, the disorder potentials of different islands are uncorrelated. In the case of long-range interactions with $d/r^{isl}=0.5$, correlations are maximal when $i=j$, but they do not vanish for $i\neq j$. $\langle \phi_i^{\rm dis} \phi_k^{\rm dis} \rangle$ is finite for at least $|i-k|\leq 3-4$. The correlation of disorder decays faster than the interactions, as shown in the figure. The correlations between $\phi_i^{\rm dis}$ and its nearest neighbors $\phi_{i\pm 1}^{\rm dis}$ make it more likely for the disorder potential differences $\Phi_i^{\rm dis}$ to have small magnitudes.

V. LONG-RANGE INTERACTIONS: TRANSPORT

A. Threshold

When the interaction strength between charges at the nanoparticle and those at the electrodes does not vanish for any particle the polarization potential drop at every junction is finite. In a clean array, the potential gradient created by this polarization potential drop allows current once an electron-hole pair is created and the threshold voltage equals the minimum voltage, which allows the creation of an electron-hole pair. This differs from what was found in the purely on-site case.

The cost in energy to create an electron-hole pair in junction i in an uncharged array is $\Delta E = E_i^{e-h} - \Lambda_i^\alpha V$. We can define a junction dependent threshold voltage for creating an electron-hole pair $V_i^{{\rm TH},\alpha} = E_i^{e-h}/\Lambda_i^\alpha$. In the onsite limit $V_i^{{\rm TH},\alpha}$ is finite only at one or both contact junctions and infinite at the bulk but with long-range interactions $V_i^{{\rm TH},\alpha}$ is finite at every junction. Due to the smaller value of the excitonic energy and the larger potential drop $V_i^{\rm TH}$ is smallest at the contact junctions.

Figures 12(a) and 12(b) show the dependence of the threshold voltage V_T of clean, symmetrically biased arrays with long-range interactions on N and on the spacing between array sites, d/r^{isl}. The threshold voltage is determined by Λ_1^α and Λ_{N+1}^α, which give the polarization potential drops at the contact junctions. V_T increases sublinearly with increasing N and eventually saturates. As the spacing between the leads increases, the polarization potential drop at each contact junction decreases until eventually it reaches a minimum value at which the polarization of each contact is only due to the interaction of each contact with the lead closest to it. For N and d/r^{isl} large enough that the polarization potential drop across the contacts is not strongly influenced by interactions with the opposite lead, decreasing the nanoparticle spacing decreases the polarization potential drop across the contact junctions and the threshold increases. For N and d/r^{isl} small enough that both leads strongly influence the polarization of both contact junctions, decreasing d/r^{isl} increases the polarization potential drop at the contact junctions and the threshold decreases. The potential drops and threshold can be estimated by using an unscreened r^{-1} model for the inverse capacitance elements associated with the leads, $C_{i,0}^{-1}$ and $C_{i,N+1}^{-1}$. These estimates are included as the dashed lines in Figs. 12(a) and 12(b).

As shown in the inset of Fig. 12(b) V_T changes smoothly with α, contrary to the peak-valley structure found in the onsite interaction case. The threshold voltage is less dependent on α as N increases and as d/r^{isl} decreases because the

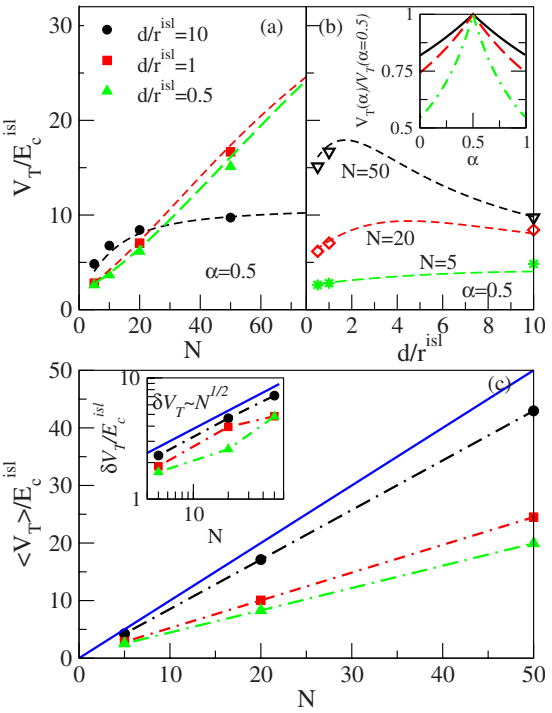

FIG. 12. (Color online) (a) and main figure in (b): With symbols it is respectively plotted the threshold voltage V_T of symmetrically biased arrays $\alpha=0.5$, with no disorder as a function of number of islands N and of array spacing d/r^{isl} for the inverse capacitances calculated as described in the Appendix. The threshold voltage of clean arrays is controlled by the value Λ_i^α at the contact junctions. The dashed lines are estimates for V_T that use a r^{-1} interaction to approximate the polarization potential drops across the contact junctions Λ_1^α and Λ_{N+1}^α. Inset in (b): Threshold voltage of clean arrays for several array parameters as a function of α normalized to the value for a symmetrically biased array. From top to bottom $d/r^{isl}=0.5, N=50$, $d/r^{isl}=0.5, N=20$, and $d/r^{isl}=10, N=50$. (c) Main figure: Average threshold voltage of disordered arrays versus the array length at three different array spacings. The solid line shows the dependence of the average threshold on array length in the limit of onsite interactions. The inset shows the root-mean-square deviation of the threshold voltage distribution. For small d/r^{isl} it deviates from the $N^{1/2}$ dependence found in the onsite case (solid line). In inset and main figure dashed-dot lines are a guide to the eye and same legend as in (a) applies

applied voltage drops more homogeneously across the array junctions. This dependence disappears completely if the polarization potential drops linearly. In this last case the threshold voltage of clean arrays would be $V_T=(N+1)E_c^{isl}$.

In the charge disordered onsite case every up step in the disorder potential prevents current flow and has to be compensated by a charge gradient. In the long-range case up steps in the disorder potential drop can localize the charge only if its value is larger than the polarization potential drop at the same junction. Due to the polarization voltage drop at the bulk, the threshold junction can be other than the contact ones. In some cases with a finite polarization drop at a junction, which is slightly smaller than the energy cost for tunneling a small increase in the voltage in the electrodes permits the tunneling. Increasing the voltage above the minimum bias voltage, which permits the generation of electron-hole pairs, will in the cases with small disorder potential at the junction result in a negative potential drop at the given junction and allows the flow of charges. However, quite often, the entrance of more charges and the creation of a charging potential gradient is required as in the onsite case. The interaction between charges in different islands decreases the energy for the entrance of charges with opposite sign and increases the one for the entrance of charges with the same sign. This effect was attributed to an attraction (repulsion) between the injected soliton and an antisoliton (soliton) on the array by Bakhalov *et al.*[48] Accumulation of charges in the array increases the threshold voltage. On the other hand, a value of $\phi_i^{\rm dis}$ at the contact islands favorable for the entrance of charge unto the array can decrease it, as the polarization potential drop to allow entrance of charge is smaller. Both mechanisms compete to determine V_T. For large d/r^{isl} the accumulation of charges is more important as the voltage drop at the bulk junctions is small and on average V_T of large arrays will increase compared to the clean array threshold voltage. On the contrary the second effect can be more important for small d/r^{isl}.

Numerically we have found a linear dependence of the threshold voltage on the number of particles in the array [see Fig. 12(c)]. Decreasing the array spacing decreases the average thresholds below the threshold values of the arrays in the on-site limit. Only at the largest array spacing ($d/r^{isl}=10$) studied we recover the dependence of the fluctuations of the threshold voltage on array length predicted by Middleton and Wingreen[31] [see inset of Fig. 12(c)].

B. Flow of Current

1. Voltages close to threshold

In the onsite interaction case the linearity of current close to threshold is due to the bottleneck character of one of the junctions and the linear dependence of the energy for tunneling of the bottleneck process on the bias voltage. These two assumptions remain valid for long-range interactions and a linear $(V-V_T)$ dependence is also found. In the case of clean arrays, the threshold and low-voltage bottleneck for current are found at the contact junctions and

$$I \sim \frac{\Lambda_{1,N+1}^\alpha}{R_{1,N+1}}(V-V_T). \tag{31}$$

This equation can be obtained equating the current to the tunneling rate at the contact junction, which acts as a bottleneck, as discussed in Sec. III B. For $\alpha=1/2$, for which $\Lambda_1^{1/2}/R_1$ and $\Lambda_{N+1}^{1/2}/R_{N+1}$ have to be added in the expression for the slope. Dependence on N, d/r^{isl}, and α via the dependence of $\Lambda_{1,N+1}^\alpha$ on these parameters is found as seen in Figs. 13(a) and 13(b). The value of Λ_i^α, which appears in the expression of V_T, is the same that controls the linearity of the IV curves very close to threshold. The behavior of the slope of I vs $(V-V_T)$ with α, N, and d/r^{isl} is opposite to the one of V_T. For $\alpha\neq 1/2$, increasing N and decreasing d/r^{isl} decreases the slope because these changes reduce the contact junctions polarization drop. For the same reason, biasing the array in a

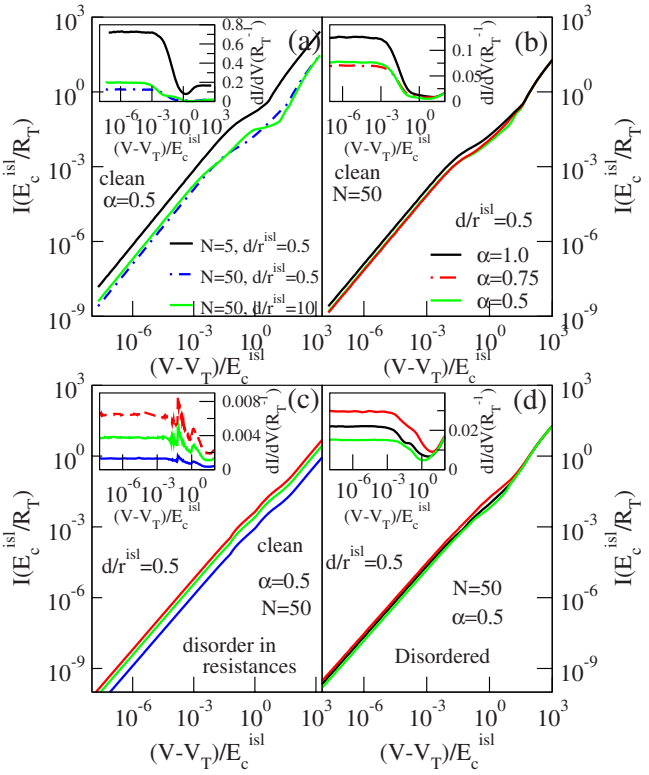

FIG. 13. (Color online) *I-V* curves of ordered arrays with long-range interaction at voltages very close to threshold. The insets show the derivatives of the *I-V* curves. As in the case with onsite interactions very close to threshold the *I-V* is linear. The linear regime ends at voltages $V-V_T \sim 10^{-2}E_c^{isl}$, much lower than the values used in experiments to check the power-law dependence close to threshold. (a) shows how varying the length and spacing of symmetrically biased arrays modifies the slopes of the linear regimes due to the change in the polarization potential drop factors Λ_i^α and correspondingly the fraction of potential, which drops in the junction which acts as bottle-neck. (b) In a similar way, the slope depends on how symmetrically the array is biased. (c) plots the *I-V* curves and derivatives corresponding to clean arrays with equal length d/r^{isl} and α but different junction resistances. Resistances in these plots vary randomly in between $(5-11)R_T$, $(8-21)R_T$, and $23-83R_T$ in top, middle, and lower curves. (d) *I-V* curves corresponding to three different realizations of charge-disordered arrays with all junction resistances equal $N=50$ and $\alpha=0.5$. Contrary to what was found for onsite interactions the slope of the low-voltage linear current can be different for arrays with the same nominal parameters if there is charge disorder. This reflects that the bottleneck is not necessarily a contact junction but can be a junction in the bulk.

more asymmetric way [increasing $(|\alpha-1/2|)$] changes the slope. The slope also depends on the junction resistances, as in the case with on-site interactions [see Fig. 13(c)].

In Fig. 13(d), we plot the current and its derivative with respect to voltage for several configurations of disorder corresponding to the same value of d/r^{isl}, N, and α and the same junction resistances. Contrary to the onsite case, the slope depends on the charge-disorder configuration. With long-range interactions, the above-threshold bottleneck (and below-threshold current blocking) junction is not necessarily either of the contact junctions but depends on the particular disorder configuration. The slope of the linear dependence can then be controlled by Λ_i^α with $i \neq 1, N+1$. The slope is generally larger (smaller) when the bottleneck junction lies closer to the edge (middle) of the array. Changing α also modifies the slope of the disordered case, not shown. This modification can be due to the change of λ_i^α with or without a change in the bottleneck junction.

2. Intermediate voltage regime

As in the on-site case, the linearity of the current disappears when the bottleneck description stops being valid. This happens at very small values of $(V-V_T) \sim 10^{-2}E_c^{isl}$. To show how this situation leads to sublinear behavior let us assume that the transport happens through a sequence of $N+1$ tunneling processes and consider a bottleneck process with rate $\Gamma_i = R_i^{-1}\Lambda_i^\alpha \tilde{V}$ with $\tilde{V}=V-V_T$ and another process in the sequence with rate $\Gamma_j = R_j^{-1}(E_j^T + \Lambda_j^\alpha \tilde{V})$. Here E_j^T is the gain in energy of the second process at $V=V_T$. If these two processes have rates much smaller than the rest of processes in the sequence, the current can be approximated by

$$I \sim \frac{1}{\tau_i + \tau_j} = \frac{R_i^{-1}\Lambda_i^\alpha \tilde{V}}{1 + \dfrac{R_i^{-1}\Lambda_i^\alpha \tilde{V}}{R_j^{-1}(E_j^T + \Lambda_j^\alpha \tilde{V})}} \sim R_i^{-1}\Lambda_i^\alpha \tilde{V}\left(1 - \frac{R_i^{-1}\Lambda_i^\alpha \tilde{V}}{R_j^{-1}E_j^T}\right). \tag{32}$$

The slope of the current and the lost of linearity depend on the resistance of the junctions, as discussed in the on-site case. In the clean long-range case, comparing the values of Λ_i^α the linear behavior lasts longer in shorter arrays, smaller d/r^{isl} and smaller α, as in these cases the values of Λ_i^α are more homogenous throughout the array. The disordered long-range case is more complex. Due to the nonhomogeneous increase in polarization voltage drop a junction, which has a small energy gain can increase this gain more than other junctions when the applied voltage increases and the dependence of the slope with the array parameters is not so easily predicted.

Above the linear regime there is a region of smoothed steps in the *I-V* curve. Decreasing d/r^{isl} smooths the steps, and for small d/r^{isl}, they are hardly distinguishable. This behavior is seen in Fig. 14(a), which compares the onset of current at voltages not extremely close to threshold for several array parameters. For clarity the curves have been plotted as a function of $(V-V_T)$. The staircase profile differs in all these cases. The top curve corresponds to an $N=50$ array with onsite interactions. In this case to allow current flow a charge gradient at each bulk junction has to be created but once charge can enter the array it flows easily through it producing sharp onset of the current close to threshold. The steps at higher voltages are just barely visible at this scale. For long-range interactions, the polarization voltage at each junction is finite and it is not necessary to create a charge gradient at the inner junctions and the steps' shape is modified. The three bottom curves correspond to $d/r^{isl}=10$. Several features can be appreciated in these curves. The step shape is clearly seen. As the potential drop at the inner junc-

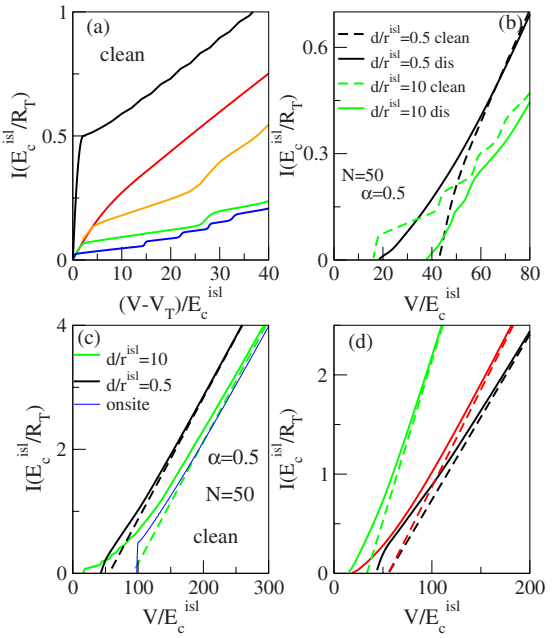

FIG. 14. (Color online) In (a) and (b) the *I-V* characteristics show the Coulomb staircase and correspond to arrays with homogeneous resistances. (a) From top to bottom, the first four curves correspond to $\alpha=0.5$ and respectively to $N=50$ with onsite interaction; $N=50$ with $d/r^{isl}=0.5$; $N=30$ with $d/r^{isl}=10$; $N=50$ with $d/r^{isl}=10$. The lowest curve corresponds to a $N=50$ and $\alpha=1$ and $d/r^{isl}=10$. The threshold voltage has been subtracted. V_T equals 98, 43, 14, 16, and 9.7, respectively. In the onsite case it is necessary to create a charge gradient at every junction to allow current, but once charge can reach the opposite electrode it flows easily and the *I-V* shows a large jump close to threshold. For $d/r^{isl}=10$ a charge gradient is not created and bulk junctions slow the current flow producing the staircase structure. The step width is smaller for forward bias $\alpha=1$ than for symmetric bias, but contrary to the behavior found in the Coulomb staircase for onsite interactions with long-range interactions the step width is not fixed. The steps are washed out for $d/r^{isl}=0.5$ due to a more homogeneous polarization potential drop through the array. (b) *I-V* curves for disordered arrays with $d/r^{isl}=0.5, 10$. The clean case is included for comparison. (c) *I-V* in a large voltage scale for clean arrays with homogeneous resistances; from top to bottom the solid lines correspond to $d/r^{isl}=0.5$, $d/r^{isl}=10$ and on-site interactions. The dashed lines give the asymptotic predictions for $d/r^{isl}=0.5$ and 10. At high voltages all the curves have the same slope given by R_{sum}^{-1}. The offset voltages differ as the excitonic energies do. (d) *I-V* curves in a large voltage scale corresponding to $d/r^{isl}=0.5$ symmetrically biased arrays. From top to bottom $N=30$ and $N=50$ disordered arrays with homogeneous resistances and a $N=50$ clean array with the first resistance ten times larger than the other ones. The dashed lines give the asymptotic predictions. The slopes of both $N=50$ curves differ, but their offset voltages are the same.

tion is small, bulk junctions control the flow of current at each plateau and their slope is small. The slope is larger for shorter arrays. The step width depends on the value of α, as also found for on-site interactions. Contrary to the short-range case, the step width is not a constant throughout the curve as the presence of charges in the array influences the energy cost to add charges from the electrodes to the first or last island. For small d/r^{isl} the polarization potential drop at the inner junction is larger and the charges flow more easily. In Fig. 14(b) we can see the different *I-V* curves in clean and disordered arrays. Especially interesting is the disordered $d/r^{isl}=0.5$ *I-V* characteristic. It looks superlinear, similar to what would be found if a power-law larger than unity is present at these voltages. We have observed that this approximate superlinear-type dependence is common in disordered arrays with small d/r^{isl}. If experimentally the power-law behavior expected close to threshold is measured at these voltages (larger than those at which the linear behavior is predicted), the exponent of the power-law could be erroneously assigned a value larger than one.

3. Linear behavior at high voltages

Expression (21) is not restricted to on-site interactions and applies also in the long-range limit. The slope of the current does not depend on the range of the interaction or the presence of charge disorder but the offset voltage at which the asymptotic expression cuts the zero current axis does[64,65] via the value of E_i^{e-h}. In Figs. 14(c) and 14(d) numerical results are compared with the asymptotic behavior predicted by Eq. (21). In Fig. 14(c) *I-V*'s for symmetrically biased arrays with $N=50$ nanoparticles and different interaction range are plotted. At high voltages slopes are equal but the offset voltages to which they extrapolate are not. Note the difference between the value of threshold and the one of the offset. In particular, the $d/r^{isl}=10$ curve has a smaller threshold and larger offset than the $d/r^{isl}=0.5$. In Fig. 14(d) the influence of the number of junctions and their resistance in the high-voltage current are reported and shown to be in good agreement with the approximate prediction.

C. Voltage drop

With long-range interactions in a clean array, V_T is given by the minimum bias voltage, which allows the creation of an electron-hole pair. Very close to V_T the voltage drop reflects the polarization drop $\Lambda_i^\alpha V$ at each junction. The potential drop distribution depends on the length of the array N, the bias asymmetry α, and on the range of the interactions d/r^{isl}. This dependence is confirmed in Figs. 15(a) and 15(b) where the potential drop is plotted for different array parameters. The value of Λ_i^α is included for comparison in Fig. 15(b). The voltage drop is very different from the one found in the onsite case [included in the inset of Fig. 15(a)], where in the bulk it is due to charge accumulation at the islands. The dependence on the value of the resistance is extremely weak even once the polarization potential drop is subtracted (not shown) and not observable, except if the difference in the value of resistances is very large. In the disordered case with long-range interaction in some cases once charge is allowed to enter the array it can flow. Then the average potential drop is approximately the sum of the disorder potential and the polarization potential. In general, when this happens the threshold voltage is smaller than the one in the clean case as the disorder potential reduces the polarization potential drop necessary in at least one of the contact junctions. For large d/r^{isl} it is more probable that one or more charges

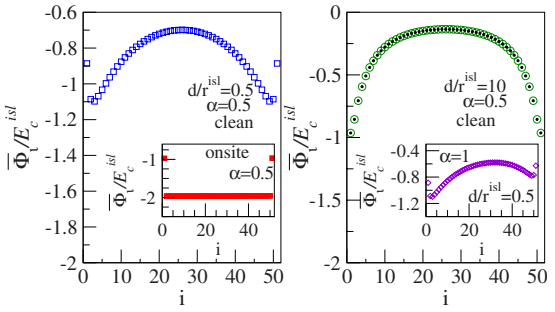

FIG. 15. (Color online) Average voltage drop close to threshold for $N=50$ clean arrays with different parameters. Main figures are for $\alpha=0.5$ and long-range interaction. The average potential drop essentially equals the polarization potential for each value of d/r^{isl}, which is plotted as filled small dots in (b) for comparison. This behavior contrasts with the potential due to the charge gradient, which has to be created in the onsite case, shown in the inset of (a). As shown by comparing main figure in (a) with the inset in (b), a change in the value of α modifies the potential drop through the array.

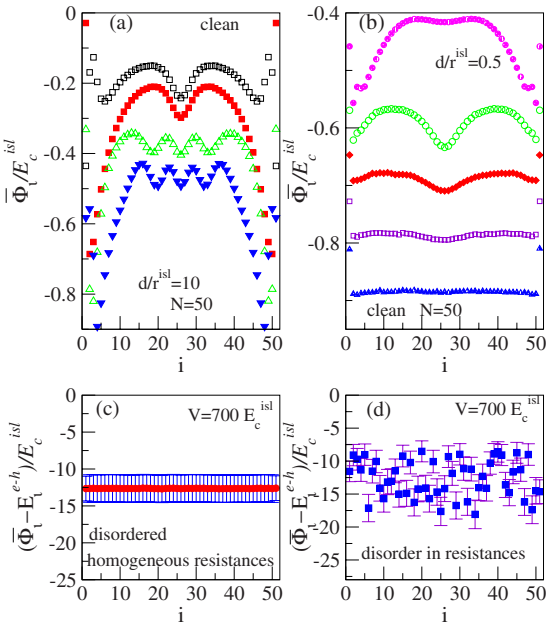

FIG. 16. (Color online) Average potential drop at the array junctions at intermediate (upper figures) and high voltages (lower figures) for $\alpha=0.5$ and $N=50$. Upper figures correspond to clean arrays. Curves in (a) are for $d/r^{isl}=10$ and (from top to bottom) $V=20,32,44,56E_c^{isl}$. The oscillations in average potential found in the on-site case at intermediate bias voltages are still present, and the number of maxima increases in two when going to a higher step. In (b) $d/r^{isl}=0.5$ and $V=46,60,70,80,90E_c^{isl}$. The number of maxima has not increased in this range of voltages but oscillations are smoothed with increasing bias voltage. In spite of the large value of the voltage the current is still in the first step of the Coulomb staircase [see Fig. 5(a)]. The potential drop at $V=90E_c^{isl}$ resembles the one at high voltages, homogeneous except by the excitonic term responsible of the offset. In (c) and (d) the excitonic energy has been subtracted from the average potential drop at high voltages. Once this term is subtracted the average potential drop is completely homogeneous through the array in (c) where there is charge disorder, and all resistances are equal but not in (d), which corresponds to a clean array but with resistances which vary randomly between $(5-11)R_T$.

remain stacked in the array, similar to the case with on-site interactions and the charge potential due to these stacked charges has to be added.

At intermediate voltages, in the Coulomb staircase regime, a similar behavior to the one found in the onsite case is observed in Fig. 16(a) corresponding to a clean array and $d/r^{isl}=10$. In Fig. 16(b) corresponding to $d/r^{isl}=0.5$ for all the voltages plotted, the number of maxima is 2, and their amplitude decreases until at the largest voltage oscillations cannot be discerned. Comparing with Fig. 14 one realizes that the step number has not changed. The *I-V* curve reaches the high-voltage regime without showing stepwise behavior.

At high voltages, the potential drop is qualitatively similar to the one found in the on-site case. The voltage drops linearly only after subtracting from each junction the excitonic energy. Some examples of this behavior are shown in Fig. 16. In Fig. 16(c) we can see that as expected, in the absence of resistance disorder, once the excitonic energy is subtracted the potential drops homogeneously through the array even if there is charge disorder, while it is proportional to the resistance value when resistances are not homogeneous, as in Fig. 16(d).

VI. SUMMARY OF RESULTS

In summary, we have studied the electronic transport at zero temperature through an array of N metallic islands with quantized charges placed in between two large electrodes, the source and the drain, respectively, at voltages V_0 and V_{N+1} with $V_0-V_{N+1}=V$ and $V_0=\alpha V$. The nanoparticle level spacing was assumed negligible and the transport treated at the sequential tunneling level. The interactions between the conductors are given by an inverse capacitance matrix C^{-1}. We have considered both short (restricted to charges placed in the same island) and long-ranged interactions. For the case of long-range interactions C^{-1} includes the screening produced by the proximity of the other conductors. To determine this screening, we have developed two methods, which allow us to calculate the inverse capacitance matrix of the system under study (see Appendix).

Screening and disorder for long-range interactions. As shown in Fig. 9(a), the effect of screening starts to be relevant when $d/r^{isl}\sim 1-2$, there is no divergence in the value of C_{ii}^{-1} at small d/r^{isl} values, but capacitance values and their inverses saturate at finite values. As discussed previously by Matsuoka and Likharev[69] for the case of cylindrical nanoparticles, the interaction between charges is reduced, with respect to the $1/r$-law, only when the nanoparticles are very close, at larger distances the interaction increases and approaches the $1/r$ law from above, resulting in a bump in the interaction potential when compared to Coulomb law [see Fig. 9(b)]. In the Appendix, we relate this antiscreening effect to the dipolar charges induced in the conductors.

Long-range interactions screen the disorder potential and induce correlations between the values of ϕ_i^{dis} on different

islands. The distribution of the island and junction potentials is modified in comparison to the one found for on-site interactions. The maximum and minimum values of $\{\phi_i^{\text{dis}}\}$ and $\{\Phi_i^{\text{dis}}\}$ are given by $\pm C_{ii}^{-1}/2$ and E_i^{e-h}. These effects are shown in Figs. 10 and 11.

Threshold. In the purely onsite interaction limit for clean symmetrically biased arrays the threshold voltage V_T equals $2NE_c^{isl}$ for odd N and $2E_c^{isl}(N-1)$ for even N. The even-odd effect disappears for forward biasing ($\alpha=1,0$) and $V_T=E_c^{isl}(2N-1)$ [see Fig. 1(a)]. The dependence on the number of nanoparticles differs qualitatively of the dependence predicted for weakly coupled islands[52] because in the purely onsite case a charge cannot flow freely through an empty and clean array and a charge gradient at the junctions has to be created to allow the flow of current. The threshold voltage is not affected by disorder in the junction resistances but it depends on the selected disorder configuration if charge disorder is present. With charge disorder, the average threshold voltage is independent of α and we recover previously predicted values $V_T=E_c^{isl}N$ [see Fig. 1(b)].

With long-range interactions, the polarization potential drop across the array creates a potential gradient which facilitates charge flow. In clean arrays, V_T is the minimum voltage that allows the creation of an electron-hole pair [see Figs. 12(a) and 12(b)]. In the disordered case, two effects compete that can increase or decrease the threshold voltage compared to the clean case. Charge accumulation can be induced by up-steps in the disorder potential, increasing V_T, and the disorder potential distribution can reduce the energy to create an electron-hole pair decreasing it. The latest effect dominates for small d/r^{isl} [see Fig. 12(c)].

Current power-law dependence close to threshold. At voltages very close to threshold, current depends linearly on $(V-V_T)$. This dependence has been obtained both numerically and analytically and resolves previous controversy on the power-law close to threshold. The linear behavior occurs because the junction through which charges enter into the array acts as a bottle neck. The range of voltages at which this linear dependence holds is probably too small to be observed experimentally. Linearity is lost when the tunneling rate through the contact junctions is comparable to the tunneling rate of other processes. In the short-range case, Fig. 2, the slope is independent of the number of nanoparticles N but depends on the resistance of the contact junctions and on the bias parameter α. With long-range interactions, Fig. 13, the slope depends on the resistance of the bottle-neck junction, which is not necessarily at the contacts. Since the slope also influenced by the way in which the polarization voltage drops through the array it depends on α and the number of particles.

Current in the Coulomb staircase regime. The linear regime is followed by a Coulomb staircase at intermediate voltages. The staircase profile depends on the junction resistances values. For onsite interactions, see Fig. 3, the width of the steps depends on α and on the presence of charge disorder. For clean arrays the bias voltage step width is $2E_c^{isl}$ for forward bias and $4E_c^{isl}$ for symmetric bias. The step width changes if disorder is present but still depends on the value of α. With long-range interactions, the steps are smoother than in the onsite case [see Figs. 14(a) and 14(b)]. Contrary to the onsite case, due to the interaction between the charges in different islands, the width of the steps is not fixed.

Linear regime at high voltages. At high voltages the current depends linearly on the bias voltage. The asymptotic *I-V* characteristic is given by Eq. (21) and cuts the zero current axis at a finite offset voltage [see Figs. 4 and 14]. The high-voltage linear behavior is reached for bias voltages V_{linear} approximately three times larger than the offset. V_{linear} can be very large in long arrays. The slope of the asymptotic linear *I-V* is given by the inverse of the sum of the junction resistances in series. The offset voltage is given by the sum of the excitonic energies of all the junctions and its value depends on the range of the interaction.

Potential drop. In the bottleneck regime in the short-range case, the potential drop reflects the charge accumulation at the islands, necessary to create the potential gradient through the array which allows the flow of charge [see Fig. 6]. The effect of disorder in resistances is extremely weak, except for the case of symmetrically biased arrays with even number of particles. On the contrary for long-range interactions, the voltage drop through the array close to threshold reflects the polarization contribution Λ_i^{α} due to the electrodes, as shown in Fig. 15.

In the on-site case in the Coulomb staircase regime, the potential drop at the junctions shows almost periodic oscillations in disorder-free arrays, which reflect the correlated motion (see Fig. 7). Such periodicity is destroyed by charge or resistance disorder in Fig. 8. With long-range interactions, as shown in Fig. 16 at intermediate voltages an oscillatory voltage drop through the array, similar to the one found for short-range interactions is found for large values of d/r^{isl}. For small d/r^{isl} there is some remanence of this behavior but the amplitude of the oscillations can vanish while still being in the weakly defined first step of the Coulomb staircase.

At large voltages, the potential drop is similar for short and long-range interactions. Proportionality between the potential drop and the junction resistance is only recovered if the excitonic energy is subtracted, as seen in Eq. (23) and Figs. 5 and 16. The mean value of the potential drop serves to compute the *I-V* characteristic in this regime.

In this work we consider transport at the sequential tunneling level. Cotunneling processes in which more than one electron can tunnel simultaneously, are expected to influence the transport at voltages of the order of this threshold or smaller. In the presence of cotunneling current will not vanish at zero temperature and finite voltages, but it can be very small in long arrays. The influence of cotunneling processes will be larger in arrays with smaller junction resistances.

ACKNOWLEDGMENTS

We thank S. Wehrli for useful discussions. Financial support from the Swiss National Foundation, NCCR MaNEP of the Swiss National Fonds, the Spanish Science and Education Ministry through Ramón y Cajal contract and FIS2005-05478-C02-01 grant, and the Dirección General de Universidades e Investigación de la Consejería de Educación de la Comunidad de Madrid and CSIC through Grants No. 200550M136 and No. CG07-CSIC/ESP-2323 is gratefully

acknowledged. Work at UT Austin was supported by the Welch Foundation by the NSF under Grant No. DMR-0606489 and by the ARO under Grant No. W911NF-07-1-0439.

APPENDIX: METHODS TO COMPUTE THE CAPACITANCE MATRIX

In this appendix, we discuss the two methods that we have used to calculate the interaction strength $C^{-1}_{\gamma\beta}$. The first method is an iterative and *a priori* can be used to determine the capacitance matrix $C_{\gamma\beta}$ for any geometric configuration of spheres. Although the algorithm for generating images is straightforward, the number of images required to calculate $C_{\gamma\beta}$ makes the numerical implementation of this technique nontrivial. While computer memory problems can be solved, the computation time is too large to tackle those cases with very large arrays and electrodes and small distance between conductors. On the other hand, small errors in $C_{\gamma\beta}$ can be enhanced in $C^{-1}_{\gamma\beta}$. The second method is specially useful and fast for systems with azimuthal symmetry as the one considered here. The interaction matrix $C^{-1}_{\gamma\beta}$ is calculated directly taking into account the symmetry of the system and the properties of spherical harmonics. Results obtained with both methods are in extremely good agreement.

1. Image charges method

The method of images[71] is the placement of imaginary charges inside the spheres at positions that make the potential everywhere on the surface of the conductor equal a constant. The charge Q_γ induced on a conductor in the presence of K equipotentials at potentials V_β is given by the capacitance matrix $C_{\gamma\beta}$,

$$Q_\gamma = \sum_{\beta=1}^{K} C_{\gamma\beta} V_\beta. \tag{A1}$$

The inverse capacitance matrix which enters the free energy (2) is the inverse of the capacitance matrix $C_{\gamma\beta}$.

To determine the positions of the image charges, we exploit two properties of spheres. The surface of an sphere of radius R can be set to a potential V by placing an image at the center of the sphere of charge $q=VR$. Second, if a charge q_R is located at the outside point, at a distance d_c from the center, an image charge q_I placed at the inside a distance R^2/d_c from the center in the radial line, with charge

$$q_I = -q_R \frac{R}{d_c} \tag{A2}$$

will set the potential to zero everywhere on the surface of the sphere. We determine the $(N+2)\times(N+2)$ capacitance matrix, column by column, by determining the set of image charges that sets the potentials of the spheres to $V_\alpha = \delta_{\alpha\beta}$. The capacitance matrix elements $C_{\alpha\beta}$ are given by the sum of all the charges in sphere α. To set the potential of the β sphere, with radius R_β to one, we place a charge with magnitude R_β at the center of this sphere x_β. The remaining spheres are grounded by placing images inside each sphere with charges

$$q_\nu = -\frac{R_\nu q^{\text{old}}}{|x_{q_{\text{old}}} - x_\nu|} \tag{A3}$$

at positions

$$x_{q_\nu} = x_\nu + \frac{R_\nu^2}{x_{q_{\text{old}}} - x_\nu}. \tag{A4}$$

Here q^{old} and $x_{q_{\text{old}}}$ are the value and the position of the charge which creates the inhomogeneous potential that we want to compensate and R_ν and x_ν are the radius and position of the center of the sphere to which we add the image charge q_ν. These image charges are added to all the spheres except the one in which q_{old} is placed. The charges that have been added generate new inhomogeneous potentials at the rest of the spheres and have to be compensated following the same method. This process repeats iteratively for all the charges added to all the spheres. During each iteration n, the number of new images required to compensate the potential of the other spheres approximately equals $(N+1)^n$. We eliminate some of the images by discarding images with a magnitude that is smaller than a suitable cutoff value, q_{cutoff}. We required q_{cutoff} to be small enough that the relative differences between the matrix elements generated with the cutoff value q_{cutoff} and by a larger cutoff value $q'_{\text{cutoff}}=10q_{\text{cutoff}}$ are less than one percent.

2. High-order multipoles method

Following Wehrli *et al.*,[72] the energy of the system, given by Eq. (2) can be rewritten in terms of the higher-order multipolar charges induced by the charges on the conductors as

$$F = \frac{1}{2} \sum_{\alpha,\beta,l,m,l',m'} Q^{\alpha,*}_{l,m} G^{\alpha\beta}_{l,m,l',m'} Q^{\beta}_{l'm'}. \tag{A5}$$

Here the Greek indices denote the conductors, l and l' denote the order of the multipole, and $m=-l,\ldots,l$ and $m'=-l',\ldots,l$ denote the azimuthal number. This matrix G is Hermitian with respect to the exchange of α,l,m and β,l',m'. Using the linear-response form for the induced multipoles, the higher-order multipolar charges, $Q^\alpha_{l,m}$, can be expressed in terms of the (monopolar) charges on the conductors $Q_\gamma = Q^\gamma_{00}$ as

$$Q^\alpha_{l,m} = \sum_\gamma \Gamma^{\alpha\gamma}_{l,m} Q_\gamma. \tag{A6}$$

Substituting Eq. (A6) into Eq. (A5) and comparing it with Eq. (2), the inverse capacitance matrix can be expressed as

$$C^{-1}_{\gamma\eta} = \sum_{l,m,l',m',\alpha,\beta} G^{\alpha\beta}_{l,m,l,m'} \Gamma^{\alpha\gamma *}_{l,m} \Gamma^{\beta\eta}_{l',m'}. \tag{A7}$$

The order of approximation in this method is the number of the highest multipoles l,l' included. The multipolar charge induced is the one which minimizes the energy. Separating the monopolar contribution $(l,m=0)$ in the expression of the free energy and minimizing the latter with respect to $Q^\alpha_{l,m}$, we obtain

$$\mathbf{Q}_A = -\hat{G}_{AB}^{-1}\hat{G}_{B0}\mathbf{Q}_0. \tag{A8}$$

Here $A=l,m$ and $l\neq 0$, correspondingly B, and the equation is written in vectorial and matrix notation. In terms of the $\hat{G}$ matrices,

$$\hat{C}^{-1} = \hat{G}_{00} - \hat{G}_{0A}\hat{G}_{AB}^{-1}\hat{G}_{B0}. \tag{A9}$$

Matrix $\hat{G}_{00}$ has dimension $N_s \times N_s$ with N_s the total number of conductors. Matrices $\hat{G}_{0A}$ and $\hat{G}_{B0}$ are $N_s \times (N_s N_{\text{totalmulti}})$ and $(N_s N_{\text{totalmulti}}) \times N_s$, respectively, and matrix $\hat{G}_{AB}$ has dimension $(N_s N_{\text{totalmulti}}) \times (N_s N_{\text{totalmulti}})$. $N_{\text{totalmulti}}$ is the maximum number of multipolar terms considered. Formally it is

$$N_{\text{totalmulti}} = \sum_{l=1,l_{\max}} (2l+1), \tag{A10}$$

with $l_{\max}$ the order of the maximum multipole included in the approximation. However, the symmetries of the problem can help us to reduce it as the $\hat{G}_{AB}$ elements corresponding to certain m_l can be seen to vanish by symmetry. Depending on the geometry of the conductors it can be convenient to use different number of $l_{\max}$ for different conductors. In particular, in the case of an array of small islands sandwiched by two large electrodes, it is better to use a larger number of multipoles at the electrodes. The expression for $G_{lm}^{\alpha\beta}$ follows from the decomposition of $1/|\mathbf{a}-\mathbf{b}-\mathbf{R}|$, with $\mathbf{a}$, $\mathbf{b}$, and $\mathbf{R}$ as the three points in space and depends on the geometry of the conductors. For $\alpha \neq \beta$

$$G_{l_1 m_1 l_2 m_2}^{\alpha\beta} = \left[\frac{(l_1+l_2-m_1-m_2)!\,(l_1+l_2-m_1+m_2)!}{(l_1+m_1)!\,(l_1-m_1)!\,(l_2+m_2)!\,(l_2-m_2)!}\right]^{1/2} \times (-1)^{l_2+m_2} I_{l_1+l_2+m_1-m_2}(x_\beta - x_\alpha), \tag{A11}$$

with $I_{l,m}$ the irregular solid spherical harmonics,

$$I_{lm}(\mathbf{r}) = \frac{1}{r^{l+1}}\sqrt{\frac{4\pi}{2l+1}}Y_{\text{lm}}(\Omega). \tag{A12}$$

The sign of $G_{l_1 m_1 l_2 m_2}^{\alpha\beta}$ depends not only on l_2 and m_2 but also on the order $\alpha\beta$ or $\beta\alpha$ through the dependence of $I_{l_1+l_2+m_1-m_2}(x_\beta - x_\alpha)$.

For the case of an sphere α with radius R_α, $G_{l_1,m_1,l_2 m_2}^{\alpha\alpha}$,

$$G_{l_1 m_1 l_2 m_2}^{\alpha\alpha} = \delta_{m_1 m_2}\delta_{l_1 l_2}\frac{1}{R_\alpha}^{2l_1+1}. \tag{A13}$$

The case of spheres on a row is especially simple. There is azimuthal symmetry and all terms with $m\neq 0$ vanish. Thus at order $l_{\max}$, $N_{\text{totalmulti}}=l_{\max}$. This simplification allows us to go to reasonably high orders. Most of the cases presented here are done with $l_{\max}\sim 8$. We can eliminate the indexes m_1, m_2 from the matrix G. Together with the diagonal terms $G^{\alpha\alpha}$ calculated above and using that

$$Y_{l0} = \sqrt{\frac{4\pi}{2l+1}}P_l(\cos\,\theta), \tag{A14}$$

and $P_l(1)=1$ and $P_l(-1)=(-1)^l$ the equations are greatly simplified. Thus

$$G_{l_1,l_2}^{\alpha\beta} = \frac{(l_1+l_2)!}{l_1!\,l_2!}(-1)^{l_1}\frac{1}{r_{\alpha\beta}^{l_1+l_2+1}}, if x_\beta > x_\alpha,$$

$$G_{l_1,l_2}^{\alpha\beta} = \frac{(l_1+l_2)!}{l_1!\,l_2!}(-1)^{l_2}\frac{1}{r_{\alpha\beta}^{l_1+l_2+1}}, if x_\beta < x_\alpha \tag{A15}$$

for $\alpha\neq\beta$. Here $r_{\alpha\beta}$ is the distance between the centers of the spheres α and β. The diagonal of G_{0A} and G_{A0} is zero and $G_{0A}^{\alpha\beta}=G_{A0}^{\beta\alpha}$. Note that

$$G_{00}^{\alpha\alpha} = \frac{1}{R_\alpha}, \tag{A16}$$

$$G_{00}^{\alpha\beta} = \frac{1}{r_{\alpha\beta}}. \tag{A17}$$

The zero-order approximation recovers our expectation for the case of far-apart spheres. The correction to the inverse capacitance due to the higher-order multipoles is given by $-\hat{G}_{0A}\hat{G}_{AB}^{-1}G_{B0}$. As spheres come closer, higher-order terms become more and more important. This is reasonable taking into account that the interaction between two multipolar charges $Q_{l_1 m_1}^{\alpha}$ and $Q_{l_2 m_2}^{\beta}$ decays as $r_{\alpha\beta}^{l_1+l_2+1}$.

From the decomposition of the induced screening charge in high-order multipoles, it is possible to get some insight on how does the bump discussed in Sec. IV appear. Let δC^{-1} be the correction to the inverse capacitance due to screening and consider $\delta C_{\alpha\beta}^{-1}$, with $0<\alpha<\beta<N$, calculated to dipolar order. The sign of correction terms coming from the charge induced in conductors from 1 to $\alpha-1$ and from $\beta+1$ to N_s is opposite to the one coming from conductors $\alpha+1$ to $\beta-1$ contribute to δC_{α}^{-1} with different sign. As further are these conductors to α and β, the correction will be smaller. Individual contributions from each conductor γ will be larger when $\alpha<\gamma<\beta$. The contribution of the interaction term, which comes from the dipoles generated in conductors between α and β, increases $C_{\alpha\beta}^{-1}$. Only when the contribution of the terms, which decrease the inverse capacitance matrix element, is able to compensate the contribution of those ones which increase it, the total change will be negative. As closer are α and β the number of terms increasing the interaction decreases. $C_{\alpha\beta}^{-1}$ is expected to be smaller than the bare value, only if α and β are very close, which results in the appearance of the bump and the antiscreening effect at intermediate and large distances.

*leni@icmm.csic.es

[1] R. L. Whetten, J. T. Khoury, M. M. Alvarez, S. Murthy, I. Vezmar, Z. L. Wang, P. W. Stephens, C. L. Cleveland, W. D. Luedtke, and U. Landman, Adv. Mater. (Weinheim, Ger.) **8**, 428 (1996).

[2] C. P. Collier, R. J. Saykally, J. J. Shiang, S. E. Henrichs, and J. R. Heath, Science **277**, 1978 (1997); G. Markovich, C. P. Collier, S. E. Henrichs, F. Remacle, R. D. Levine, and J. R. Heath, Acc. Chem. Res. **32**, 415 (1999).

[3] R. Parthasarathy, X.-M. Lin, and H. M. Jaeger, Phys. Rev. Lett. **87**, 186807 (2001).

[4] J. D. Le, Y. Pinto, N. C. Seeman, K. Musier-Forsyth, T. A. Taton, and R. A. Kiehl, Nano Lett. **4**, 2343 (2004).

[5] Y. Lin, A. Böker, J. He, K. Sill, H. Xiang, C. Abetz, X. Li, J. Wang, T. Emrick, S. Long, Q. Wang, A. Balazs, and T. P. Russell, Nature (London) **434**, 55 (2005).

[6] K. Elteto, X.-M. Lin, and H. M. Jaeger, Phys. Rev. B **71**, 205412 (2005).

[7] J. Zhang, Y. Liu, Y. Ke, and H. Yan, Nano Lett. **6**, 248 (2006).

[8] T. P. Bigioni, X.-M. Lin, T. T. Nguyen, E. I. Corwin, T. A. Witten, and H. M. Jaeger, Nat. Mater. **5**, 265 (2006).

[9] J. Liao, L. Bernard, M. Langer, C. Schönenberger, and M. Calame, Adv. Mater. (Weinheim, Ger.) **18**, 2803 (2006).

[10] S. S. Mark, M. Bergkvist, X. Yang, L. M. Teixeira, P. Bhatnagar, E. R. Angert, and C. A. Batt, Langmuir **22**, 3763 (2006).

[11] C. B. Murray, C. R. Kagan, and M. G. Bawendi, Science **270**, 1335 (1995).

[12] D. V. Talapin, E. V. Shevchenko, A. Kornowski, N. Gaponik, M. Haase, A. L. Rogach, and H. Weller, Adv. Mater. (Weinheim, Ger.) **13**, 1868 (2001).

[13] N. Y. Morgan, C. A. Leatherdale, M. Drndíc, M. V. Jarosz, M. A. Kastner, and M. Bawendi, Phys. Rev. B **66**, 075339 (2002); V. J. Porter, T. Mentzel, S. Charpentier, M. A. Kastner, and M. G. Bawendi, *ibid.* **73**, 155303 (2006).

[14] D. Yu, C. Wang, B. Wehrenberg, and P. Guyot-Sionnest, Phys. Rev. Lett. **92**, 216802 (2004).

[15] H. E. Romero and M. Drndic, Phys. Rev. Lett. **95**, 156801 (2005).

[16] T. Feng, H. Yu, M. Dicken, J. R. Heath, and H. A. Atwater, Appl. Phys. Lett. **86**, 033103 (2005).

[17] S. Sun, C. B. Murray, D. Weller, L. Folks, and A. Moser, Science **287**, 1989 (2000).

[18] C. T. Black, C. B. Murray, R. L. Sandstrom, and S. Sun, Science **290**, 1131 (2000).

[19] V. F. Puntes, P. Gorostiza, D. M. Aruguete, N. G. Bastus, and A. P. Alivisatos, Nat. Mater. **3**, 263 (2004).

[20] F. X. Redl, K.-S. Cho, C. B. Murray, and S. O'Brien, Nature (London) **423**, 968 (2003).

[21] A. E. Saunders and B. A. Korgel, ChemPhysChem **6**, 61 (2005).

[22] E. V. Schevchenko, C. V. Talapin, N. A. Kotov, S. O'Brien, and C. B. Murray, Nature (London) **439**, 55 (2006).

[23] *Single Charge Tunneling*, NATO Advanced Studies Institute, Series B: Physics, edited by H. Grabert and M. H. Devoret (Plenum, New York, 1992), p. 294.

[24] P. Sheng and B. Abeles, Phys. Rev. Lett. **28**, 34 (1972); P. Sheng, B. Abeles, and Y. Arie, *ibid.* **31**, 44 (1973); J. S. Helman and B. Abeles, *ibid.* **37**, 1429 (1976).

[25] J. J. Shiang, J. R. Heath, C. P. Collier, and R. J. Saykally, J. Phys. Chem. B **102**, 3425 (1998).

[26] S.-H. Kim, G. Medeiros-Ribeiro, D. A. A. Ohlberg, R. S. Williams, and J. R. Heath, J. Phys. Chem. B **103**, 10341 (1999); J. F. Sampaio, K. C. Beverly, and J. R. Heath, *ibid.* **105**, 8797 (2001).

[27] I. S. Weitz, J. L. Sample, R. Ries, E. M. Spain, and J. R. Heath, J. Phys. Chem. B **104**, 4288 (2000).

[28] B. M. Quinn, I. Prieto, S. K. Haram, and A. J. Bard, J. Phys. Chem. B **105**, 7474 (2001).

[29] R. C. Doty, H. Yu, C. K. Shih, and B. A. Korgel, J. Phys. Chem. B **105**, 8291 (2001).

[30] A. Courty, A. Mermet, P. A. Albouy, E. Duval, and M. P. Pileni, Nat. Mater. **4**, 395 (2005).

[31] A. A. Middleton and N. S. Wingreen, Phys. Rev. Lett. **71**, 3198 (1993).

[32] K. A. Matsuoka and K. K. Likharev, Phys. Rev. B **57**, 15613 (1998); D. M. Kaplan, V. A. Sverdlov, and K. K. Likharev, arXiv:cond-mat/0303477 (unpublished).

[33] M. Shin, S. Lee, K. W. Park, and E. H. Lee, Phys. Rev. Lett. **80**, 5774 (1998).

[34] D. M. Kaplan, V. A. Sverdlov, and K. K. Likharev, Phys. Rev. B **65**, 193309 (2002).

[35] D. M. Kaplan, V. A. Sverdlov, and K. K. Likharev, Phys. Rev. B **68**, 045321 (2003).

[36] Y. A. Kinkhabwala, V. A. Sverdlov, and K. K. Likharev, J. Phys.: Condens. Matter **18**, 2013 (2006).

[37] R. Kotliar and S. Das Sarma, Superlattices Microstruct. **20**, 641 (1996).

[38] I. S. Beloborodov, A. V. Lopatin, V. M. Vinokur, and K. B. Efetov, Rev. Mod. Phys. **79**, 469 (2007); I. S. Beloborodov, A. Glatz, and V. M. Vinokur, Phys. Rev. B **75**, 052302 (2007); T. B. Tran, I. S. Beloborodov, X. M. Lin, T. P. Bigioni, V. M. Vinokur, and H. M. Jaeger, Phys. Rev. Lett. **95**, 076806 (2005).

[39] A. Altland, L. I. Glazman, and A. Kamenev, Phys. Rev. Lett. **92**, 026801 (2004); J. S. Meyer, A. Kamenev, and L. I. Glazman, Phys. Rev. B **70**, 045310 (2004).

[40] Y. L. Loh, V. Tripathi, and M. Turlakov, Phys. Rev. B **72**, 233404 (2005).

[41] K. B. Efetov and A. Tschersich, Europhys. Lett. **59**, 114 (2002).

[42] J. Zhang and B. I. Shklovskii, Phys. Rev. B **70**, 115317 (2004).

[43] D. S. Novikov, B. Kozinsky, and L. S. Levitov, Phys. Rev. B **72**, 235331 (2005).

[44] M. M. Fogler, S. V. Malinin, and T. Nattermann, Phys. Rev. Lett. **97**, 096601 (2006).

[45] R. Parthasarathy, X.-M. Lin, K. Elteto, T. F. Rosenbaum, and H. M. Jaeger, Phys. Rev. Lett. **92**, 076801 (2004); K. Elteto, E. G. Antonyan, T. T. Nguyen, and H. M. Jaeger, Phys. Rev. B **71**, 064206 (2005).

[46] K. C. Beverly, J. F. Sampaio, and J. R. Heath, J. Phys. Chem. B **106**, 2131 (2002); F. Remacle, C. P. Collier, G. Markovich, J. R. Heath, U. Banin, and R. D. Levine, *ibid.* **102**, 7727 (1998); F. Remacle, K. C. Beverly, J. R. Heath, and R. D. Levine, *ibid.* **106**, 4116 (2002).

[47] A. S. Cordan, A. Goltzené, Y. Hervé, M. Mejías, C. Vieu, and H. Launois, J. Appl. Phys. **84**, 3756 (1998); A. Pépin, C. Vieu, M. Mejias, Y. Jin, F. Carcenac, J. Gieraz, C. David, L. Couraud, A. S. Cordan, Y. Leroy, and A. Goltzené, Appl. Phys. Lett. **74**, 3047 (1999); A. S. Cordan, Y. Leroy, A. Goltzené, A. Pepin, C. Vieu, M. Mejias, and H. Launois, J. Appl. Phys. **87**, 345 (2000); Y. Leroy, A. S. Cordan, and A. Goltzené, *ibid.* **90**, 953 (2001).

[48] N. S. Bakhalov, G. S. Kazacha, K. K. Likharev, and S. I. Serdyukova, Sov. Phys. JETP **68**, 581 (1989).

[49] S. Semrau, H. Schoeller, and W. Wenzel, Phys. Rev. B **72**, 205443 (2005).
[50] M. G. Ancona, W. Kruppa, R. W. Rendell, A. W. Snow, D. Park, and J. B. Boos, Phys. Rev. B **64**, 033408 (2001).
[51] A. Bezryadin, R. M. Westervelt, and M. Tinkham, Appl. Phys. Lett. **74**, 2699 (1999).
[52] G. Y. Hu and R. F. O'Connell, Phys. Rev. B **49**, 16773 (1994).
[53] J. A. Melsen, U. Hanke, H. O. Müller, and K. A. Chao, Phys. Rev. B **55**, 10638 (1997).
[54] C. A. Berven and M. N. Wybourne, Appl. Phys. Lett. **78**, 3893 (2001).
[55] C. Kurdak, A. J. Rimberg, T. R. Ho, and J. Clarke, Phys. Rev. B **57**, R6842 (1998).
[56] S. Jha and A. A. Middleton, arXiv:cond-mat/0511094 (unpublished).
[57] C. Reichhardt and C. J. Olson Reichhardt, Phys. Rev. Lett. **90**, 046802 (2003).
[58] Some previous work on capacitance disorder can be found in Refs. 53 and 56.
[59] Y. Xue and M. A. Ratner, Phys. Rev. B **68**, 235410 (2003).
[60] M. Stopa, Phys. Rev. B **64**, 193315 (2001).
[61] D. V. Averin and K. K. Likharev, in *Mesoscopic Phenomona in Solids*, edited by B. L. Altshuler, P. A. Lee, and R. A. Webb (Elsevier, Amsterdam, 1991).
[62] M. Amman, R. Wilkins, E. Ben-Jacob, P. D. Maker, and R. C. Jaklevic, Phys. Rev. B **43**, 1146 (1991).
[63] A. E. Hanna and M. Tinkham, Phys. Rev. B **44**, 5919 (1991).
[64] U. Geigenmüller and G. Schön, Europhys. Lett. **10**, 765 (1989).
[65] N. S. Bakhalov, G. S. Kazacha, K. K. Likharev, and S. I. Serdyukova, Physica B (Amsterdam) **173**, 319 (1991).
[66] J. L. Sample, K. C. Beverly, P. R. Chaudhari, F. Remacle, J. R. Heath, and R. D. Levine, Adv. Mater. (Weinheim, Ger.) **14**, 124 (2002).
[67] In Ref. 31 the average threshold voltage is predicted to be linear on the number of junctions, which in our case is $N+1$. It is straightforward to argue for both $\alpha=1,1/2$ that $\bar{V}_T$ is linear in the number of bulk islands N as observed in Fig. 1(b). In large arrays the difference between both predictions is negligible.
[68] D. N. Tsigankov, E. Pazy, B. D. Laikhtman, and A. L. Efros, Phys. Rev. B **68**, 184205 (2003).
[69] K. K. Likharev and K. A. Matsuoka, Appl. Phys. Lett. **67**, 3037 (1995).
[70] C. B. Whan, J. White, and T. P. Orlando, Appl. Phys. Lett. **68**, 2996 (1996).
[71] W. R. Smythe, *Static and Dynamic Electricity* (McGraw-Hill, New York, 1950).
[72] S. Wehrli, E. Koch, and M. Sigrist, Phys. Rev. B **68**, 115412 (2003).